QATAR UNIVERSITY

Graduate Studies

College of Arts and Sciences

PHYSICO-MECHANICAL PROPERTIES OF NEW ELECTROSPUN POLYVINYLIDENE FLUORIDE NANOCOMPOSITES

A Thesis in Materials Sciences and Technology

By Ahmed Abdel Atty Issa Ramadan

Submitted in Partial Fulfillment

of the Requirements

for the Degree of

Master of Science/Arts

June 2015

Declaration

To the best of my knowledge, this thesis contains no material previously published or written by another person or institution, except where due reference is made in the text of the thesis. This thesis contains no material which has been accepted for the award of any other degree in any university or other institution.

Name: Ahmed Abdel Atty Issa Ramadan

Signature: Date:

COMMITTEE

The thesis of **Ahmed Abdel Atty Issa Ramadan** was reviewed and approved by the following:

We, the committee members listed below accept and approve the thesis/dissertation of the student named above. To the best of this committee's knowledge, the thesis/dissertation conforms to the requirements of Qatar University, and we endorse this thesis/dissertation for examination.

Name __ Prof. Mariam Al-Maadeed ______

Signature _______________________________________ Date__________

Name __ Prof. Adriaan Stephanus Luyt____

Signature _______________________________________ Date__________

Name __ Dr.Mabrouk Ouederni __________

Signature _______________________________________ Date__________

Name ___Dr.Khaled Mohamed Youssef ___

Signature _______________________________________ Date__________

Abstract

This study aimed to prepare and characterize poly(vinylidene fluoride) (PVDF) nanofibres with the following additives: graphene oxide (GO), cellulose, and silver nanoparticles (Ag-NPs). Two types of solvents were used to prepare the virgin and composite materials: acetone and DMF, which lead to a porous surface of the nanofibres. Effect of combination of the additives and effect of two salts (sodium chloride and tetraethyl ammonium chloride) was also considered. These nanofibers were produced by electrospinning technique. The properties of the prepared samples were studied by scanning electron microscope, differential scanning calorimeter, Fourier transform infrared, X-ray diffraction , thermal gravimetric analyzer, tensile test instrument , dynamic mechanical analyzer, and dielectric analyzer.

The objective of this study is to improve the crystallinity percentage and especially the beta phase content in the produced nanofibers which is important to improve the properties for different applications such as energy harvesting.

Ag-NPs improved the smoothness and reduced the thickness of the nanofibres due to the increase in conductivity but upon increasing the concentration to more than 1.4% agglomeration occurred and polydispersed fibres are produced. Improvement of the crystallinity percentage was achieved to a maximum at the following percentage 0.3% GO, 0.5% cellulose, and 0.4% Ag-NPs with crystallinity percentage of 50%, 43.2% and 45.4% respectively, these values are higher than the 41.7% of the PVDF nanofibres. The same additives percentage increased the thermal stability of the nanofibres (with exception of cellulose which had a shift to 1% rather than 0.5%)

Combination of fillers lowered the crystallinity percentage compared to single additives due to the heteronucleation effect of the fillers. Enhancement in the beta phase was achieved at the following concentrations of the additives 0.1% GO, 1% cellulose and 0.2% of Ag-NPs. The nanocomposite became less compact as the 2Θ shift to lower values.

Improvement in storage modulus was achieved with the addition of 0.3% of GO due to the stiffness of GO sheets. The similar effect was achieved with the addition of 0.5% of cellulose and

0.2% of Ag-NPs, but due to the polymer chains are entrapped in agglomeration of the particles, and cannot move freely.

Loss modulus had a considerable low value when 0.7% of GO was added to the PVDF which showed improved mechanical energy distribution within the material.

The relative permittivity of PVDF/GO, PVDF/cellulose, and PVDF/Ag-NPs is improved with addition of the fillers, it was around 50 % at low frequency, this improvement could be due to the Maxwell-Wagner-Sillar (MWS) interfacial polarization.

Table of Contents

LIST OF FIGURES

LIST OF TABLES

ACKNOWLEDGMENT

I would like to express my sincere gratitude to my advisor **Prof. Mariam Ali AlMadeed** for the unlimited support of my thesis. Her guidance helped me in research and writing of this thesis. Beside my advisor, I would like to thank all of my advisory committee members, especially **Prof. Adriaan Stephanus Luyt** for his effort in correction, encouragement and insightful comments.

My sincere thanks and gratitude to my colleagues in Chemistry & Earth Science department for their encouragements, especially **Prof. Hala Al-easa**. Also, all members of Materials Sciences and Technology program, Central lab Unit, Center for advanced Materials, Gas Processing Center for their support, special thanks to Dr. Miroslav Mirlik , Mrs. Elzabeth Jacob and Mr.Mostafa Al-Ghoul for their experimental support.

The financial fund **QUST-CAM-FALL-14\15-1** grant from the office of Research at Qatar University is highly appreciated.

DEDICATION

I dedicate my work to my parents, there are no words that can express my thanks to them as they had unlimited support and inspiration during my life, I ask Allah to be in good health all the time.

I also dedicate this work to my wife who has supported and encouraged me during the challenges of the graduate studies.

This work is also dedicated to my family, for all the care.

Chapter 1. Introduction

1.1 The PVDF and PVDF composites

Poly(vinylidene fluoride) (PVDF) is a relatively low cost material with many remarkable properties such as thermal stability, high flexibility, chemical resistance, good mechanical properties and biocompatibility [1-3]. In addition, it is a piezoelectric and pyroelectric semicrystalline material with a high dielectric constant due to the presence of fluorine atoms and C-F bonds [2, 4]. A lot of work has been done to study PVDF, especially its degree of crystallinity, because PVDF presents five distinct crystalline phases related to different chain conformations. These phases are the α-, β-, γ-, ε-, and δ-phases. The beta phase is crystalline phase of the PVDF where the polymer has (TTTT) conformation. The β-phase is significant because it has the highest dipolar moment per unit cell, and hence improves its piezoelectric properties [2, 5].

Due to the unique properties of PVDF and its copolymers, they are used in many applications like water filtration, e.g. graphene oxide (GO)/PVDF composites are used to remove the natural organic materials from fresh water [3, 6]. Doping of $CoCl_2$/PVDF composites with γ-zeolite gives excellent catalytic activity in the hydrolysis of sodium borohydride ($NaBH_4$) to produce hydrogen in proton exchange membrane fuel cells [2]. PVDF has high anodic stability due to the presence of the fluorine atom, and it has the highest relative permittivity ($\varepsilon = 6$ to 12) among similar piezoelectric polymers. Recently, it gained attention in the field of lithium batteries development as electrolyte [2, 7]. It is also used in seawater desalination by membrane distillation [8]. In addition, some researchers used it in pollutants removal, acid gas desorption membranes and recovery of biofuels via evaporation, because of the mechanical properties, chemical resistance and thermal stability of this material [3]. PVDF has very good biocompatibility, so it is used as sutures and as scaffold for the cells in an implantation [9]. Many research groups work on improving the beta phase in PVDF products (by changing the type of filler, fabrication method, and post processing), so that it can be used in sensors, actuators, transducers, energy harvesting and FTIR detectors [10-14].

Although PVDF has large number of applications, the current work focuses on modifying PVDF for possible use in the energy field. PVDF has a high dielectric constant compared to other polymers, and it is easy to manipulate, in addition to the already mentioned properties. The piezoelectric properties of PVDF depend on the beta phase content and the degree of crystallinity. This work therefore aims to improve the beta phase content and the crystallinity of the produced fibers by using certain fillers such as GO, cellulose and Ag-NPs. This should lead to an improvement in the mechanical properties and thermal stability.

The selection of the fillers was done after a thorough literature review. GO has an antimicrobial effect, it enhances the beta phase, and it has good mechanical properties. Cellulose is biodegradable, low cost and available, and it enhances the beta phase content. Ag-NPs have antimicrobial effect and can enhance the conductivity.

The electrospinning technique forces PVDF molecules to align, which should enhance beta crystallization and the degree of crystallinity. This alignment is the result of three forces: (i) the shear force in the needle, (ii) the electrostatic force between the needle and the collector, and (iii) the mechanical stretching from the rotating drum. A combination of the presence of the fillers and electrospinning is used to improve the beta phase, crystallinity, and other properties.

1.2 Aims and objectives

The main target of this project was the fabrication of nanofibrous film of PVDF with a high beta phase content, improved thermal stability, and enhanced mechanical properties by using electrospinning, and the resulting material can be used for many applications such as energy harvesting, energy storage, sensors, water treatment, actuators, and artificial muscles. To achieve this goal the following objectives were formulated:

- Optimize the electrospinning conditions for PVDF nanofibers.
- Prepare PVDF composites with different fillers.
- Study the influence of filler type and its concentration on the following
    - The morphology of the produced nanofibers.
    - Degree of crystallinity and beta phase content.
    - Thermal stability.
    - Dielectric properties.
    - Mechanical properties.
- Investigate the addition of salts (sodium chloride and tetraethyl ammonium chloride) on selected physical and chemical properties of the PVDF films.
- Study the effect of mixed fillers on selected physical and chemical properties of the PVDF composite.

Chapter 2. Literature review

2.1. Poly(vinylidene fluoride)

PVDF is a fluorinated polymer which is prepared from vinylidene fluoride (CH_2-CF_2) by a free radical (or controlled radical) polymerization process using emulsion or suspension polymerization [1, 4]. The properties of a small molecule will be dramatically influenced if one hydrogen atom is replaced with a fluorine atom. This impact is much greater in the case of a polymer molecule with its much larger molecular weight.

In 1965, Makarevich and Nikitin discovered that PVDF has two phases (α and β) by using infrared spectroscopy. In 1969 Dr. Heiji Kawai discovered the piezoelectric properties of PVDF. The piezoelectric materials are a substances which produce an electricity when it is subjected to mechanical work. In 1981 Furakawa and Johnson confirmed the piezoelectric nature of PVDF and identified its Curie point as 103^{o}C. After this discovery, PVDF received a great deal of scientific attention.

Enzo Giannetti said that the presence of the fluorine atom will polarize the C-F bond and make it a partially ionic bond and strengthen the C-C bond, but there is steric hindrance of the F-atom which will decrease the C-C bond strength [4], and therefore PVDF has five different crystalline conformations that are called phases. The most common phases are the α-, β-, and γ-phase, shown in figure 2.1. In addition, there are two other phases (ε- and δ-phase). The α-phase structure has a TGTG' (trans-gauche–trans-gauche) conformation. It is not polar and does not have electro-active properties [2, 15]. The β-phase has a (TTTT) conformation, which is a zigzag structure, with a dipole moment perpendicular to the polymer chain. It shows electroactive behavior [16]. Most of the research concentrated on improving the β-phase content in the polymer [5, 15, 17]. The ϒ-phase has a (T3GT3G’) conformation, and this phase is electroactive but not as much as the β-phase. Another phase is ε-phase which is similar in structure to the γ-phase, and δ-phase to the α-phase [2]. <note :- my objective is improve the β-phase content.>

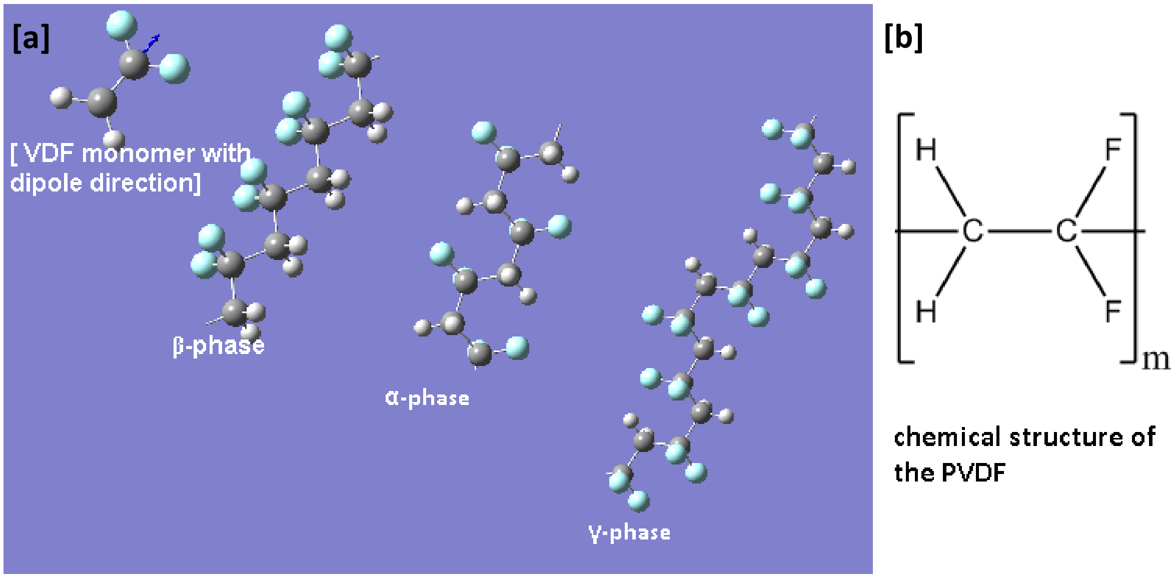

Figure 2.1 Schematic representation of vinylidene fluoride molecule,[a] the chain conformation for the α, β, and γ crystalline phases, and [b] the chemical structure of PVDF

2.2. Applications of PVDF

Due to the unique properties of PVDF, it has many applications that can be summarized as follows:

Microelectronic applications, such as **sensors and transducers,** based on the electroactive (piezoelectric, ferroelectric, and pyroelectric) properties of PVDF. The Chiu group used PVDF to fabricate a heartbeat and respiration detection system based on its piezoelectric properties [18]. Merlini et al. developed a novel pressure sensor from poly(pyrole) as a conductor coated with PVDF [19]. A number of other groups worked on the development of pressure sensors or transducers by improving the content of the β-phase in PVDF [12, 20, 21]. In some other applications, a film of PVDF is used in hydrophones (working in the range of 0.5 to 15 MHz) that are used in medical ultrasonic equipment [22]. Because of PVDF's pyro-electric properties, some research groups fabricated a membrane from it to be used as a temperature sensor in the biomedical field [23].

Micro lenses: In 2004, Bormashenko et al. worked on the development of micro lenses for FTIR from electrical poled and non-poled high molecular weight PVDF [24].

Energy harvesting: a small amount of energy (usually mechanical energy) is collected from the surrounding environment and converted to electricity. Research has been conducted to use PVDF to transform the mechanical energy from the ocean waves and from highway traffic to produce electricity [25]. Chen et al. introduced a new technique to prepare highly porous PVDF thin film to improve PVDF crystallinity, compressibility and charge collecting area [11]. Another group wrote an article review on the principles, performance issues, fabrication techniques, and characterization instruments of PVDF and zirconate/titanate nanogenerators [26]. In 2013, Pereira et al. found that the energy obtained from pure PVDF is higher than that obtained from PVDF/barium titanate due to increased mechanical stiffness, and the energy output was improved by using a smaller non-piezoelectric filler [27]. < note:- the PVDF has piezoelectric properties, in addition to pyro-electric.>

Artificial muscles and actuators: PVDF fibers or films with a considerable amount of β-phase will contract when they are subjected to an electric field. Pérez et al. used PVDF film as actuator with an attached mirror to move a laser beam in the kHz range for a high speed laser scanning system [13].

Membranes: Due to the outstanding mechanical properties and chemical resistance of PVDF, it is used extensively in membrane industries such as water filtration, desalination, gas separation, separator for lithium batteries, and etc. Such as, the ultrafiltration membranes are prepared from PVDF/GO with immersion phase inversion and improved properties at a concentration 0.2% of GO [28].

Biomedical applications: Due to the biocompatibility and mechanical properties of PVDF, it is used as sutures in surgery [9]. Klinge et al. developed a mesh from PVDF for abdominal hernia repair. They compared the PVDF mesh with polypropylene (PP) mesh, and they found that the PVDF could be a good alternative for PP due to improved biostability [29]. Damaraju et al. used PVDF as scaffold for bone generation. They studied the β-phase content and alkaline phosphatase activity, and found that there is a relation between the β-phase content and an increase in the activity of the alkaline phosphatase [30].

Traditional applications: Due to the good chemical resistance of PVDF, it is used in the manufacture of pipes for transport of chemicals, especially for acids, organic solvents and halogenated compounds. It is also used in the electric industry as insulation material for cable shielding of data transfer lines, safety & security systems, wire harness for the cars and control cables, due to the fact that the fire does not spread easily through it, and the produced smoke is minimal when it is burned. In addition, it has good resistance to ultraviolet and gamma radiations [31].

2.3. PVDF composites and additives

Most of the fillers and additives are added to improve a certain property of PVDF, such as the β-phase content, mechanical properties, antimicrobial and anti-fouling properties, hydrophilicity, or ease of processing.

Various research groups work on improving the β-content to enhance the piezoelectricity, pyro-electricity, and ferro-electricity of PVDF. Iron salts and oxides like Fe_2O_3 are used to enhance the beta phase [32, 33]. Clay nanoparticles and organoclay are used to increase the percentage of the beta or gamma phases [15, 34, 35]. Achaby et al. found that when they used 0.1% GO, the PVDF formed pure β-phase due to the interaction between the carbonyl group in GO and the fluorine atoms [36]. Li et al. found that using GO sheets increased the gamma phase [37]. Silver nanoparticles and nanowires were also used to improve the conductivity and beta phase at the same time [12]. The sensitivity of a pressure sensor was improved by adding silver nanowires [12, 38]. Cellulose can be used to improve the beta phase content due to the presence of -OH groups [5, 15]. Many other fillers like carbon nanotubes, ZnO, $BaTiO_3$, and piezoelectric ceramic were tested to enhance the beta phase content [15, 39, 40].

PVDF has good mechanical properties (its young's modulus is 2.5 GPa[41]) , but some research used fillers to improve it even more. The use of GO nano-sheets [36], silver nanoparticles [42] and multiwalled carbon nanotubes [43] were found to improve the mechanical properties of the composite at a particular concentration of each filler.

When PVDF is used in water purification as a membrane or in biomedical applications such as suture or meshes, it faces a problem of bacterial and fungal growth. Silver is a traditional antimicrobial agent, and some studies show that around 700 ppm will kill 100 % of bacteria, even drug resistant bacteria [44, 45]. Scientists also used GO as antimicrobial filler, and it was found that 40 ppm of GO will kill 90 % of E-Coli in two hours [46].

The contact angle of PVDF is close to 135^{o}, which means that it is a hydrophobic material. Some applications, however, require the PVDF to be hydrophilic, so fillers such as cellulose acetate [47], silver nanoparticles [48] and GO [6] were added to improve the hydrophilicity.

The following methods may be used to process PVDF and its composites:

Traditional methods: The mass production of large objects from PVDF is done by extrusion, injection molding, compression molding, and hot pressing.

Electrospinning: In this technique, an electrostatic force is used to derive nanofibers from a polymer solution. This technique will be explained in detail in section 2.4.

Electrospray method: The electrospinning equipment is used for this technique, but instead of using a suitable concentration and voltage to form fibers, a low concentration and voltage are used to form tiny droplets. It is observed that the droplet size and solution viscosity control the morphology of the film, and that the key to control the whole process is the solvent [49].

Phase inversion: Most membranes that are used for water treatment or gas separation are prepared by this technique. The polymer is dissolved in a primary solvent, the polymer solution is cast onto a glass substrate as a uniform film, and the polymer is then precipitated by immersing it in water or alcohol to remove the primary solvent from the prepared film. The produced film will be porous. The film properties are controlled by the primary solvent type, the concentration of PVDF, the type of precipitation solvent, and the temperature [50-52].

Spin coating: This technique is used to deposit a highly uniform film by deposition of the polymer solution on a rotating disk. This method is used to prepare films from PVDF and its copolymers with improved permittivity, energy density, and crystallinity [53, 54].

Centrifugal spinning: Nanofibers are produced by forcing the polymer solution through a tiny hole in a high speed rotating spinneret under a centrifugal force This technique has been used to fabricate highly aligned fibrous scaffolds for tissue regeneration [55].

2.4. Electrospinning

It is the most effective technique to fabricate nanofibers. It can be used to fabricate 1D, 2D, and 3D nanofiber structures, and it can be used with natural and synthetic polymers as well as polymer composites. Different architectures can be prepared by this technique [56, 57]. Most other techniques are used in research only, but this technique is used widely in research and industry.

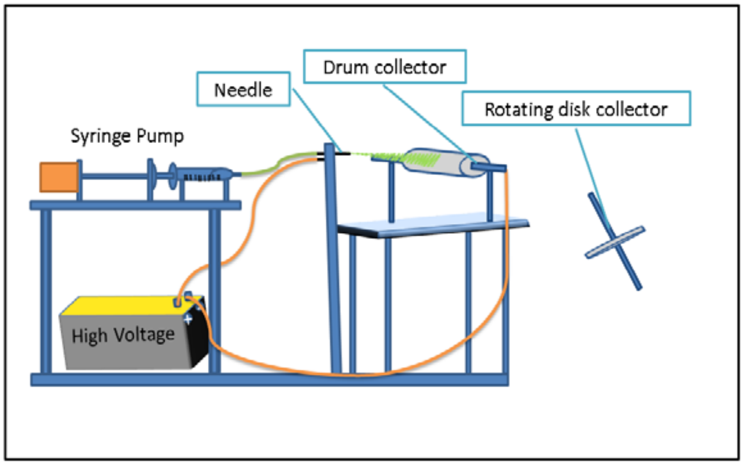

FIGURE 2.2 SCHEMATIC DIAGRAM OF ELECTROSPINNING SETUP

2.4.1. Basic setup

A typical electrospinning setup consists of three parts (see Figure 2.2). The first part is a **high voltage power supply**. One terminal of the power supply is connected to a spinneret and the other terminal is connected to a metallic collector. The voltage of the power supply ranges from 10 to 50 kV. The second part is the **spinneret**, which is a metal capillary tube, and which contains the polymer solutions or melts. The solution is fed to the spinneret at a constant and controllable rate by using a syringe pump. The third part is a ground **metal collector** which can be a flat plate, rotating drum, or rotating disc. This is usually covered in aluminum foil for ease of collection of nanofibers [58, 59].

2.4.2. The principle of work

Although electrospinning is a simple setup and straightforward technique, the physics behind it is complex. Most of the nanofiber fabrication methods are mechanical methods, but electrospinning is different as the extrusion force is generated by the interaction between the charged polymer liquid and an external applied electric field. When high voltage is applied, the polymer fluid becomes highly charged, and a solution droplet is formed at the tip under two types of forces, an electrostatic repulsion force and surface tension, and this forms a conical fluid structure called a Taylor Cone at the tip of the needle. This cone is in equilibrium until a critical potential, at which the repulsion force will overcome the surface tension, above which the solution will penetrate the Taylor cone toward the collector and the equilibrium will be destroyed. The critical potential (V_c^2) can be calculated by the Taylor equation (equation (1)).

$$V_c^2 = \frac{4H^2}{h^2}\left(\ln\left(\frac{2h}{R}\right) - 1.5\right)(1.3\pi R\gamma)(0.09) - - - - - - - - - - - - (1)$$

where H is the distance between the needle tip and the collector, h is the liquid column length, R is the outer radius of the needle, and γ is the surface tension of the fluid (the units of H, h, and R are expressed in cm, and that of γ as dyn per cm^{-1}).

Initially researchers thought that the solution go straight toward the collector, but by using many techniques such as high speed video analysis and tracer-particle tracking to track the solution from the Taylor cone to the collector, they found that the fluid goes straight for a certain distance called the critical distance (L), before making a spiral shape which is called instability elongation. The critical length can be calculated by equation (2) [56].

$$L = \frac{4KQ^3}{\pi\rho^2 I^2}(R_o^{-2} - r_o^{-2}) - - - - - - - - - - - - - - - - - - - (2)$$

where $\mathrm{R_o} = (\frac{2\sigma Q}{\pi\rho kE})^{1/3}$, Q is the flow rate, σ is the surface charge, k is the dimensionless conductivity, E is the applied electric field, I is the current passing through the jet, ρ is the liquid density and r_o is the initial radius of the jet. Equation (2) can be very useful in the near field electrospinning (NFES) technique. Equation (3) represents the classical Rayleigh instability.

$$(\varepsilon - \varepsilon')E_o^2 + \frac{4\pi^2\sigma^2}{\varepsilon'} = \frac{2\pi\gamma}{h} - - - - - - - - - - - - - - - - - (3)$$

where γ is the surface tension, h is the radius of the jet, ε and ε' are the dielectric constants, respectively inside and outside the jet, and E is the electric field. The different ES regions are illustrated in Figure 2.2.

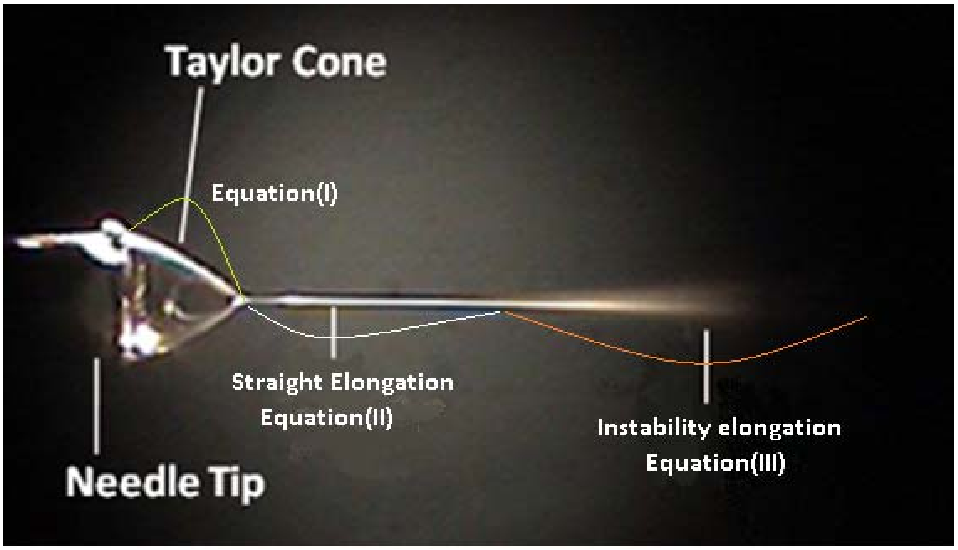

Figure 2.2 Electrospinning image showing stage formation of Taylor Cone, straight elongation, and instability elongation. Modified from [60].

2.4.3. Controlling parameters

When inspecting equations 1 to 3, we can see that there are several parameters that control the morphology and diameter of the produced nanofibers. These parameters can be divided into three categories: solution, processing, and ambient parameters. Each one of these parameters contains subcategories as was mentioned before.

3.3.3.1. Solution parameters

The most important factor is the solution viscosity, which is related to many factors, but mainly the solution concentration, the molecular weight of the polymer, as well as the conductivity, surface tension, and temperature of the solution [56]. It was, for example, found that for poly(vinyl alcohol) (PVA) a low concentration will form beads and a high concentration will form a ribbon, and that a suitable concentration to prepare good nanofiber is 6% [61, 62].

3.3.3.2. Processing parameters

They are the parameters that are related to the instrument itself and the processing method, such as the applied voltage, the distance between the spinneret and the ground collector, the rotating speed of the drum, the diameter of the spinneret (needle), and the feed rate. The applied voltage is a critical element in electrospinning. The Taylor cone will not be formed for a certain solution until the voltage exceeds the critical voltage $V_{c,}$ which can be calculated with Taylor's equation [1]. Moreover, the growth of bending instability will be affected by the applied electric field, and as a result the morphology and diameters of the nanofibers will change. Another parameter is the distance between the tip of the spinneret and the collector, because the flight time and the external electrical field that are both affected by the distance between the tip and the collector will affect the produced nanofibers. The distance should also be long enough for the elongation and drying of the fibers, otherwise beads will be formed [57, 63].

3.3.3.3. Ambient parameters

There are two ambient parameters that influence the electrospinning process. Both of them will affect the drying step in the process, which will change the morphology of the final product. The first one is **humidity**. As the humidity increases, the drying time will increase, and in some cases it will improve the morphology of the resultant nanofibers because it will give enough time for elongation before solidification. Thus nanofibers with very small diameters can be produced. In the case of poly(ethylene oxide) (PEO), it was found that as the relative humidity increased from 5.1% to 48.7%, the diameter of prepared fibers decreases from 253 to 144 nm [3]. On the other hand, some researchers observed that the fibers became thicker with increasing humidity, and that is due to neutralization of the charge on the jet which leads to the stretching force becoming too weak to elongate the fibers [62]. The second parameter is **temperature**. Increasing the temperature will lead to a decrease in the viscosity of the spinning solution. If it is highly viscous at room temperature (as in the case of the hyaluronic polymer which is a natural polyelectrolyte), it is difficult to electrospin at room temperature, hence it is electrospun at 40 ^{o}C [57]. It will also lead to a decrease in the drying time, because it will increase the solvent evaporation rate as the solution travels from the spinneret to the collector. To produce aligned nanofibers with electrospinning, the distance between the spinneret and the collector should be very small to avoid the bend instability, but then the time will not be enough to dry the nanofibers. Hence the temperature of the chamber should be increased to increase the rate of evaporation, and improve the final morphology of the nanofibers.

2.5. Aligned fiber techniques

Aligned nanofibers are important in many applications, like artificial muscles, actuators, energy storage and transportation, and in some medical applications like tissue engineering and drug delivery [64]. There are many methods used to produce aligned fibers e.g. drawing, electrospinning under customized conditions, self-assembling, and centrifugal spinning technology. Aligned fibers can be obtained from electrospinning by using certain methods such as the **rotating disk method**. In this technique the fibers are pulled out from the spinneret to a high speed rotating disk, to form aligned fibers. This technique was used to produce highly aligned nanofibers from PVDF and polystyrene solutions [64, 65]. In the **parallel plates** method the live terminal is connected to the spinneret and the ground terminal to the parallel plates, and the fibers are formed perpendicular to the plate direction in the gap between the plates. Parallel gaps in a stiff aluminum sheet instead of parallel plates were used to produce aligned fibers from poly(methyl methacrylate) (PMMA) [66]. In **near field electrospinning** (NFE), the spinneret is very close to the rotating collectors to avoid the bending instability growth stage in the formation of fibers. Nanofibers with excellent mechanical properties were prepared from MWCNT/PVDF [67] by this technique. Several research groups used **a magnetic field** during the electrospinning of Fe_3O_4 (ferromagnetic material)/polymer composites to produce aligned nanofibers [68-70].

Self-assembly (micro-patterning) : Molecules that have amphiphilic properties tend to organize themselves into ordered nanostructure shapes like micelles without any human intervention. Most of these molecules have head-and-tail-like surfactants and peptides. The heads will be organized with the heads, and the tails with tails through hydrogen bonds, electrostatic interactions, and hydrophobic forces. Fabrication by this technique is affected by the pH, concentration, and temperature of the solution. These nano-assemblies can be used in many applications like drug delivery systems or cell containers [56, 58, 59]. Iwaura et al. [71] studied the effect of sodium chloride concentration on the formation of nucleotide bolaamphiphile nanofiber, and they found that the morphology, appearance, and pH of the resultant self-assemblies strongly depend on the concentration of sodium chloride.

Phase separation is a method to prepare fibrous foam. The polymer is dissolved in a proper solvent, then the temperature is reduced to solidify the polymer (gelatinization step), and this solvent is replaced with water and the product is dried [58]. Zhao et al. used this technique to prepare Chitosan acetate nanofibers with diameters of 50 to 500 nm at different temperatures [72].

Bacterial cellulose: Some bacteria convert glucose to nanofibers, for example the acetobacter bacteria polymerize glucose as nanofiber followed by extracellular secretion [58, 59].

Templating: This is based on aluminum's unique property of self-organized pore arrays with nano-size as a result of anodization to form alumina (Al_2O_3). After filling the nano-voids with polymer, the nanofiber can be released from the alumina block by destruction of the mold [58, 59].

Drawing: Mechanical fabrication of the nanofibers by drawing viscous polymer solutions directly with mechanical tools. An example is the immersion of a glass rod in poly(trimethylene terephthalate) melt, and then moving it up to form a filament which solidifies to form nanofibers. Although this technique is very simple, it has low reproducibility and produces fibers with uncontrollable morphology. This technique can, however, be automated to prepare highly ordered patterns of nanofibers [58, 59].

Extrusion (centrifugal spinning): Extrusion is a conventional method used in textile industries, and it is not suitable to produce nanofibers without modification. However, modified extrusion methods have been developed to produce uniform fibers in the nano range by changing the die. The systems utilize air and centrifugal forces to push the polymer solutions through the die [59]. Highly aligned nanofibers were fabricated from poly(caprolactone)/gelatin composites with different ratios for medical applications by using centrifugal spinning technique [55].

Chapter 3. Materials and methodology

3. 1. Materials

All the reagents and chemicals used in this study were obtained commercially, with the exception of GO which was prepared by the modified Hummers process. Chemicals and sources are as follows: PVDF in powder form (average molecular weight 534000 amu, melting point 165^{o}C) from Sigma-Aldrich; acetone from Alfa Aesar; dimethyl formamide (DMF) from Sigma Aldrich; cellulose from Sigma Aldrich; silver nanoparticles (Ag-NPs, diameter from 20 nm to 100 nm) from Sigma Aldrich; sodium chloride from Riedel-deHaen, tetraethyl ammonium chloride (TEAC) from Fluka. GO was prepared from the following materials: Graphite powder from Sigma Aldrich, potassium permanganate from Fluka, potassium nitrate from BDH, hydrochloric acid from VWR, sulfuric acid from Breckland Scientific Supplies, hydrogen peroxide from Riedel-deHaen, and deionized water.

3. 2. Sample preparation equipment

An electrospinning machine NEU-01 with its accessories from NaBond, China was used for the preparation of all polymer films. The fabrication was carried out at room temperature and atmospheric pressure, using a standard G20 needle as the capillary. The fibers were deposited on aluminum foil covering the ground rotating drum. Each sample was electrospun until at least 4 ml of the solution was converted to fiber. All the common variables are listed in Table 3.1.

Table 3.1 Electrospinning conditions for PVDF

Parameter	**Value**
Concentration	13% w/w
Flow Rate	3 ml/h
Voltage /temp.	10.35 kV/ ambient
Distance	10 cm
Collector /speed	Drum with horizontal position of the needle/1400 rpm

3. 3. Preparation of nanofibers and nanocomposites

3.3.1. Preparation of GO

GO was prepared by using the modified Hummer method [73]. 75 ml of concentrated sulfuric acid, 1.5 g of sodium nitrate, and 3 g of graphite were mixed together and stirred in an ice bath until the temperature became around 6 °C. Then 9 g of potassium permanganate was added gradually with constant stirring. The mixture was removed from the ice bath and stirred at room temperature for one more hour. After that, 150 ml of deionized water was added gradually with continuous stirring so that the temperature did not exceed 98 °C. After the addition of water, the solution was kept on the stirrer for 15 min. 4.5 ml of hydrogen peroxide was then added to the mixture. The solution turned orange in color and was transferred to a graduated cylinder to settle. The supernatant was discarded, and the precipitate was washed with de-ionized water over multiple centrifugation cycles and finally washed with 0.1 M HCl, followed by air drying. The product was characterized by TEM, SEM, UV/Vis, XRD, TGA, and FTIR and confirmed to be GO.

3.3.2. Preparation of PVDF solution

A series of PVDF solutions were prepared with different concentrations (5%, 10%, 15%, and 20% by weight/volume) based on the work of Yee et al. [65]. A mixture of DMF and acetone in the ratio 40:60 (by weight) was used to dissolve the PVDF. These solutions were electrospun with varying electrospinning settings. The morphology of these samples was investigated by SEM to see if nanofibers were formed. After many trials, the best concentration of PVDF and electrospinning conditions for the preparation of nanofibers were selected as shown in in Table 3.1. Then the working solution (15 wt./v % PVDF)is prepared as following; 15 g of PVDF, 60 g of acetone, and 40 g of DMF were mixed and stirred for two hours at 80 °C until the solution turned completely clear. The solution at the beginning was whitish in color, then slowly turned yellow and showed an increased viscosity after a few days.

3.3.3. Preparation of PVDF composites

3.3.3.1. Preparation of PVDF/GO composites

Composites of PVDF with GO were prepared based on previous work by Liu, Wang, and Al-Achaby groups [28, 36, 46]. GO has a tendency to convert at high temperature to reduced graphene oxide (rGO) [74]. To prevent this, the PVDF/GO composite was prepared without applying of heat to GO. For this, two solutions were prepared; for solution 1, 1.5 g of PVDF, 2 g of DMF, and 6 g of acetone were mixed and stirred with heating until completely dissolved, then cooled down; for solution 2, 0.075 g of GO was dissolved in 5 g of DMF using an ultrasonic water bath, then stirred until a homogeneous solution was obtained. 2 g of solution 2 was then added to solution 1 to get PVDF/GO with a concentration of 2%. A series of dilutions of PVDF/GO were prepared with concentrations 0.1%, 0.3%, 0.5%, and 0.7 %. The solutions were then electrospun using the conditions in Table 3.1.

3.3.3.2. Preparation of PVDF/cellulose composites

This part of the work is based on previous work of the Rajesh and Bodhke groups [5, 15]. To prepare the composite, 0.107 g of cellulose fiber was dissolved in 20 g of 13% PVDF solution to give 4% cellulose with reference to PVDF. 5 g of the previous 4% solution was added to 5 g of the 13% PVDF solution to prepare a 2% cellulose solution. 2.5 g of the 4% solution was added to 7.5 g of the 13 % PVDF solution to make a 1% cellulose solution. 1.25 g of the 4% solution was added to 8.75 g of PVDF solution to make a 0.5% cellulose solution, then the composites solutions stirred overnight. The nanofiber films were then prepared by electrospinning with the settings as given in Table 3.1.

3.3.3.3. Preparation of PVDF/Ag-NPs composites

The preparation of PVDF composites with silver nanoparticles is based on the work of the Yuan, Chen, and Li groups [12, 45, 75]. PVDF/Ag-NPs solutions were prepared as follows: 0.0525 g of Ag-NPs were dissolved in 20 g of a 13% PVDF solution to prepare a 2% PVDF/Ag-NPs stock solution. The working solutions were then prepared by dilution of the stock solution with pure PVDF solution. 1, 2, 3, 4, and 5 g of the stock were diluted to 10 g with pure PVDF solution to prepare the working solutions (0.2%, 0.4%, 0.6%, 0.8%, and 1%). The solutions were electrospun with the conditions given in table 3.2.

TABLE 3.2 Electrospinning conditions for PVDF/AG-NPS

Parameter	**Value**
Concentration	0.2%, 0.4%, 0.6%, 0.8 %, and 1.0%
Flow Rate	2 ml/h
Voltage	8.0 kV (adjusted)
Distance	10 cm
Collector/speed	Rotating disk/1700-1900 rpm
Spinneret (needle)	G22

3.3.3.4. Preparation of mixtures (0.4% Ag-NPs, 0.2% GO, and 1% cellulose)

Three different mixtures were prepared from the previous stock solutions as follows:

- M1 (0.4 % Ag-NPs, and 0.3 % GO).
- M2 (0.4 % Ag-NPs, and 1.0 % cellulose).
- M1 (0.4 % Ag-NPs, 1.0 % cellulose, and 0.3 % GO).

3.3.3.5. Preparation of PVDF with sodium chloride and tetraethyl ammonium chloride (TEAC)

In this part of the practical work, the salts were selected depending on the work of the Sui and Lee groups [65, 66]. 0.5% NaCl/PVDF was prepared by adding 7.0 mg NaCl to 10 g PVDF solution. 0.5% tetraethyl ammonium chloride (TEAC) was prepared by adding 7.0 mg TEAC to 10 g of PVDF solution. Both solutions were ultrasonicated for ten minutes then stirred for 2 hours.

3. 4. Characterization and analysis techniques

The electrospun samples were analyzed with many techniques to examine their morphology and chemical/mechanical properties. The following equipment were used in this study:

3.4. 1. Differential scanning calorimetry (DSC)

DSC measures the heat flow to/from the sample to maintain the temperatures of the sample and the reference pans equal with the increasing or decreasing temperature. We can use this to determine the melting point, glass transition (T_g) and the temperature of any chemical or physical change in the sample as well as the degree of crystallinity [2, 9, 16, 32, 76, 77].

The DSC analyses were performed on a Perkin Elmer DSC4000 differential scanning calorimeter. The following equations were used to calculate the degree of crystallinity.

$$Xc = \frac{\Delta H_m}{\Delta H^o}\ x\ 100 ----------------------(4)$$

$$Xc = \left(\frac{\Delta H_m}{x\Delta H_\alpha + y\Delta H_\beta}\right) x\ 100 ---------------- (4')$$

where ΔH_m is the melting enthalpy of the sample, ΔH_α melting enthalpy of the α-phase (93.04 J/g), ΔH_β and ΔH^0 the melting enthalpies of the β-phase (103.4 J/g) and 100% crystalline PVDF (104.6 J/g), *x* and *y* are weight fractions of the α- and β-phases respectively, and which are calculated by using FTIR. Equation (4) is a simple form of equation (4'), in which it is assumed that there exists only one phase, but in reality there are at least two phases. The lamellae thickness can be calculated by the Gibbs-Thomson equation (equation (5)).

$$T_m = T_m^o\left[1 - \frac{2\sigma_e}{L\Delta H_m}\right] - - - - - - - - - - - - - - - - - - - (5)$$

where T_m is the melting temperature of the prepared sample, T_m^0 is the melting temperature at equilibrium, ΔH_m is the melting enthalpy of the polymer, L is the lamellar thickness and σ_e is the specific surface energy [78, 79].

In this experiment, the samples were scanned in two cycles at a heating rate of 10 ^oC/min, from 40 ^oC to 200 ^oC in nitrogen.

3.4. 2. Thermogravimetric analysis (TGA)

This technique was used to study the thermal stability of the materials. The samples were heated in a Perkin Elmer TGA4000 thermogravimetric analyzer from 40 ^oC to 750 ^oC at a constant rate of 10 ^oC/min in nitrogen gas, and the percentage weight loss of the samples was recorded [79].

3.4. 3. Scanning electron microscopy (SEM)

Scanning electron microscopy (SEM) has been used to study the morphology of the electrospun samples before proceeding to use other characterization techniques to confirm the preparation of the nanofibers. The surface morphology is commonly characterized by using SEM [8, 32, 80]. A FEI Quanta 200, USA scanning electron microscope was used for these analyses.

3.4. 4. Transmission electron microscopy (TEM)

The transmission electron microscope (TEM) is similar to the transmission optical microscope. Instead of using light rays, TEM uses an electron beam so it can reveal the nanoscale morphology of materials. In this work, a FEI G2 TF20, USA transmission electron microscope was used to examine the morphology of the Ag-NPs, cellulose, and GO fillers. The samples were prepared by dispersing the fillers individually in deionized water with the help of sonication, and then depositing a thin film on the TEM mesh.

3.4. 5. Attenuated total reflectance–Fourier transform infrared spectroscopy (ATR-FTIR)

FTIR is a technique which uses infrared rays to determine the chemical structure and conformation of the molecules in solid, liquid, or gaseous states. The FTIR range can be divided to three regions, near Infrared, mid infrared, and far infrared. The most common one is mid infrared due to the presence of the fingerprint region between 500 to 1500 cm^{-1}. In addition to the prediction of the chemical structure of molecules, it can be used to calculate the percentage of crystalline phases in a material, such as the calculation of the percentage of the β-phase in PVDF film.

The FTIR technique can be used to calculate the degree of crystallinity by equations (6) and (7).

$$A = \log\frac{I^{o}}{I} = LX\varepsilon - - - - - - - - - - - - - - - - - -(6)$$

where *A* is absorbance, L is the thickness of the specimen, *X is* the degree of crystallinity, ε is the molar absorptivity , I and I° are the intensities of the transmitted and incident light respectively. The percentage of β-phase in the sample is calculated by using the following equation

$$F(\beta) = \frac{A_\beta}{A_\beta + 1.26\ A_\alpha} ------------- (7)$$

where F(β) is the relative fraction of β-phase, A_β and A_α are the absorbance at 840 and 763 cm^{-1} respectively [16, 32].

In this work, the samples were scanned from 400 to 4000 cm^{-1} in a Perkin Elmer Spectrum 400 FTIR by using an ATR detector with resolution 4 cm^{-1}.

3.4. 6. X-ray diffraction (XRD)

XRD is a crystallography tool which uses X-rays to determine the crystalline phases and the intermolecular distance by using Bragg's law (equation (8)).

$$n\lambda = 2d\sin\theta ------------------ (8)$$

where n is an integer, λ is the wavelength, d is the intermolecular distance, and θ is the angle of diffraction. It can also be used to measure the grain size by using the Scherrer equation (equation (9)).

$$D = \frac{0.94\lambda}{\beta\cos\theta} -------------------- (9)$$

where D is the grain size , λ is the wavelength, β is the line broadening at half the maximum intensity after subtracting the instrumental line broadening expressed in radians, and θ is the angle of diffraction.

In this work, a Rigaku Minflix XRD was used for two purposes, first to confirm the preparation of the GO, which gave a peak at $2\theta = 10^{o}$, and second to compare the β-phase content with the results that were obtained by FTIR. The samples were scanned from 5^{o} to 45^{o}. XRD is used to differentiate between the PVDF phases, where each phase has a specific 2θ and some have more than one peak. The α-phase has four peaks at 17.66°, 18.30°, 19.90°, and 26.56°. The β-phase has one peak at 20.26°. The γ-phase has three peaks at 18.5°, 19.2°,and 20.04°. The analysis was done using a Cu-K_α (1.5406 Å) source, with applied voltage of 30 kV, current 30 mA and scan rate of 3 degree/min.

The FTIR and XRD techniques can be combined to give very clear analysis results [3].

3.4. 7. Tensile testing

A Lloyd Instruments LF plus universal tester was used to test the mechanical properties of the nanofibrous films, especially the tensile strength which is equal to the maximum stress (σ) divided by the sample cross sectional area (A). There are many mechanical properties that can be evaluated using this equipment, such as Young's modulus, strength at break, strength at yield, and elongation at break. The test was conducted at room temperature on the prepared samples. The samples were prepared in two batches: (i) samples with length 75 mm, width 5 mm, and thickness from 0.08 to 0.15 mm, and (ii) samples with length 25 mm, width 3 mm, and thickness from 0.06 to 0.068 mm. The tests were conducted with a cross-head speed of 50 mm/min with a gauge length of 25 mm.

3.4. 8. Dynamic mechanical analysis (DMA)

All polymers are viscoelastic materials, this means that they behave as a solid as well as liquid at the same time. The degree of elastic portion and a degree of viscous portion present in the material can be expressed by storage (elastic) modulus (G') or loss (viscous) modulus (G"). Using DMA, frequency dependence of both moduli can be measured, in the range of linear visoelastic region (LVR). The G' represents the energy which can be stored by the material upon mechanical stimulation and G'' represents the portion of the energy which is upon same mechanical stimulation convert to the heat and is dissipated within the material. Therefore this technique is widely used for investigation of the mechanical properties with consequences to the structural properties of the polymer materials [81].

In this work, TA Instruments RSA-G2 dynamic mechanical analyser was used to determine the G' and G". The moduli were determined in the LVR which was established at a strain deformation of γ = 0.008 % in a broad frequency range from 0.01 Hz to 100 Hz. The measured samples were in the shape of stripes with 40 mm in length, 3.5 mm in width and a similar thickness range as was mentioned in the case of tensile testing. All the measurements were performed at room temperature.

3.4. 9. Dielectric relaxation spectroscopy (DEA)

Similar approach as was used in case of DMA was applied for investigation of the dielectric properties of the sample. However, instead of the mechanical stimulus, the electrical stimulus in this case was used. Namely, the alternate current (AC) electric field of various frequencies was utilized for determination of the real and imaginary part of permittivity. After the application of the external electric field and certain frequency, the dipoles induced within the sample are able to respond to this change are represented by the relative permittivity (ε'), on the other hand the dielectric loss factor (ε'') represents amount of the dipoles which are not able to follow this changes of the electric field and thus certain amount of energy is transferred to heat dissipation. In this technique, utilizing the Novocontrol Concept 40, including the impedance analyzer, the mentioned ε' and ε'' can be evaluated as frequency dependent quantities. Samples in form of the squares with 25 mm and a thickness of 0.1 mm were measured in a broad frequency range from 10^{-1} Hz to 10^{7} Hz and an applied AC electric field of 1 V. All the measurements were performed at room temperature.

Chapter 4. Results and Discussion

The presentation of the data will be according to the following material properties: morphology, crystallinity, beta phase, thermal analysis, and mechanical properties. The effect of the following additives will be discussed: GO, cellulose fibers, Ag-NPs, and salt on selected PVDF samples.

4. 1. Morphology

4.1. 1. The morphology of the fillers

The graphene oxide (GO) filler; Figure 4.1(a) is the TEM micrograph of the prepared GO in de-ionized water, and it shows irregular GO sheets that overlay each other. Figure 4.1(b) shows smooth and large layers of GO sheets with few cracks, due to the GO was prepared without using ultra-sonication [46, 74].

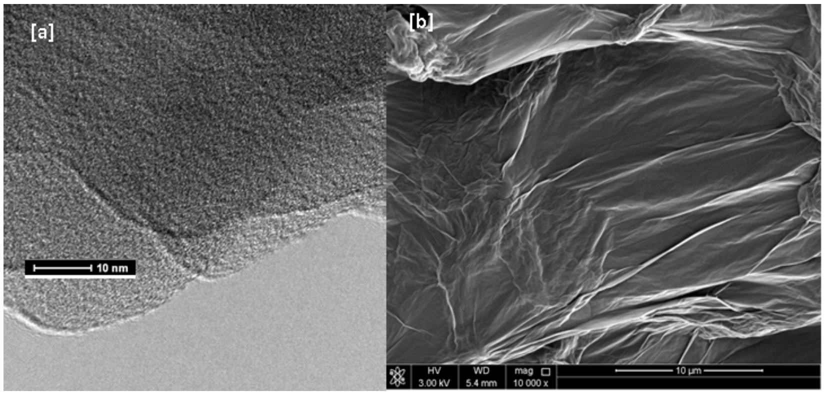

Figure 4.1 [a] TEM micrograph of GO solution in water and [b] SEM micrograph of GO film

The cellulose filler; Figure 4.2(a) shows a SEM micrograph of the cellulose filler; it shows the cellulose particles have irregular shapes with different sizes. The sizes of the cellulose particles ranged between 1 and 40 μm, but most of the particle sizes lie between 1 and 10 μm, with a maximum at 3 μm (Figure 4.2(c)).

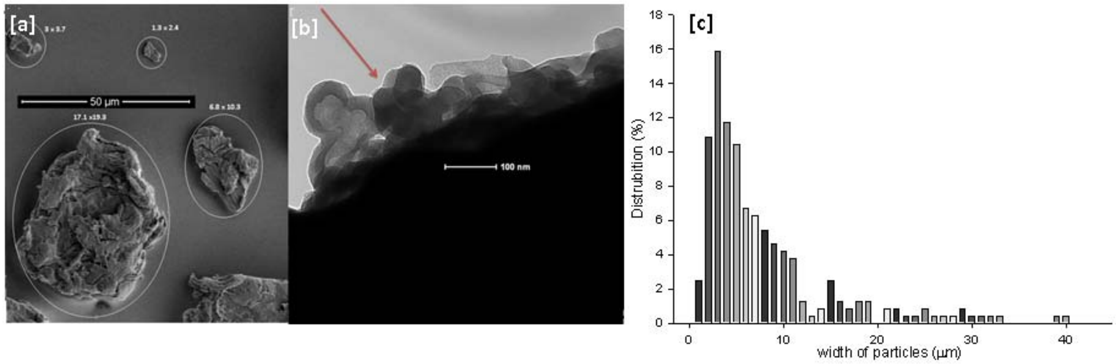

Figure 4.2. [a] SEM micrograph, [b] TEM micrograph, and [c] distribution of cellulose filler width

The TEM micrograph shows that the surface of the cellulose particles are not smooth; the surface of the particles has cilia from cellulose (Figure 4.2(b)).

<u>The silver nanoparticles (Ag-NPs) filler;</u> Figure 4.3 shows selected SEM and TEM micrographs of Ag-NPs. The SEM micrograph shows that the Ag-NPs are not completely spherical, and their diameters range from 20 to 70 nm. However, some of the particles look bigger than 100 nm because they are agglomerations of small particles (Figure 4.3(a)). The TEM micrograph shows the aggregation of Ag-NPs in the DMF solvent [45]. This will play an important role in the properties of the PVDF/Ag-NPs nanofibers [45, 48].

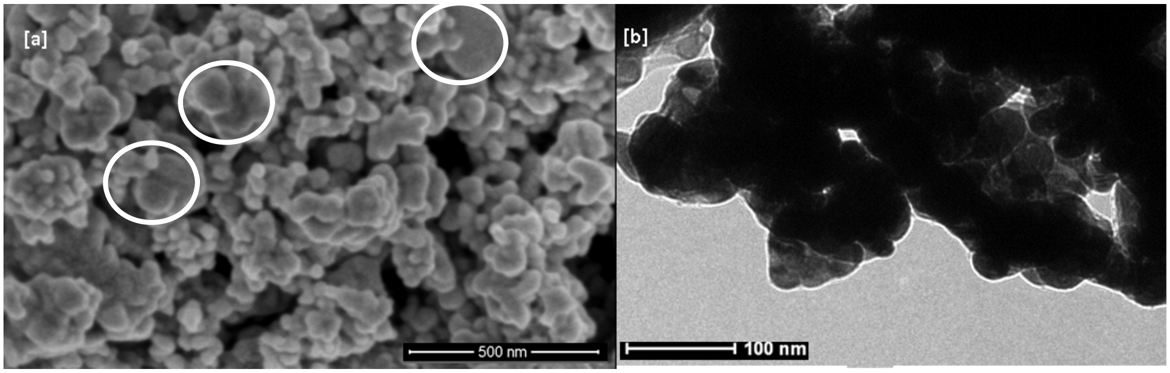

Figure 4.3. [a] SEM and [b] TEM micrographs of Ag-NPs in DMF solvent

4.1. 2. Results from drum collector

The PVDF electrospun nanofibrous films were prepared with optimized conditions as in Table 3.1, and with a concentration of 13 wt.% of PVDF. The fibers were nonwoven, nonaligned, no beads were formed, and they had diameters varying between 370 and 870 nm. The thickness of the electrospun film was not uniform, and it was observed to be thick and dense at the front of the spinneret (needle) and it became thinner away from the needle as seen in Figure 4.4. It was found that the most critical parameter in the electrospinning process is the type of solvent, because it (i) determines the dependence of the viscosity on the concentration of the electrospinning solution, and it (ii) controls the solidification step of nanofibres. Other research groups used different solvents that varied from pure DMF and dimethylacetamide (DMAc) to mixtures of DMF and acetone, or DMAc and acetone, with different ratios [45, 63, 82, 83]. In this work the DMF/acetone mixture was used to control the evaporation during the electrospinning.

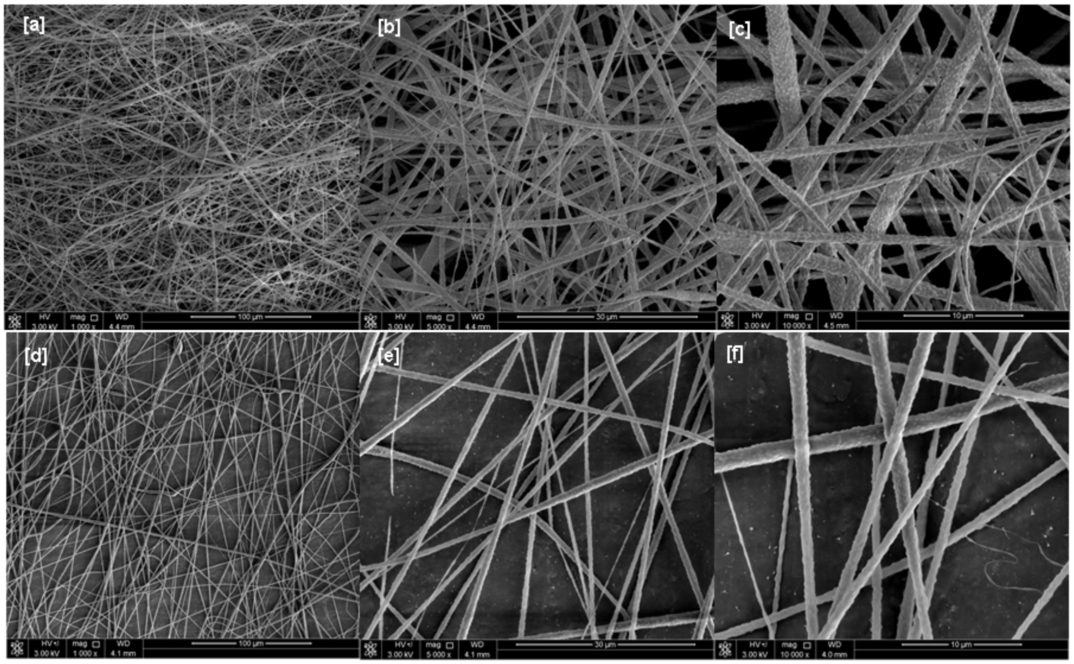

Figure 4.4 SEM micrographs of PVDF with different magnifications (a, b, c) next to the needle and (d, e, f) 5 cm away from the needle

Figure 4.5(a) shows that the fiber surfaces are not smooth but rough and porous. This is due to the usage of two different solvents in the solution, acetone (which has a boiling point at 56 ^{o}C) and DMF (which has a boiling point at (152 ^{o}C), that will evaporate at different temperatures during electrospinning, which causes the formation of the observed porous structure. In addition, the thick fibers have a more porous and rough surface than the thin fibers, because the large fibers can trap the solvent for a longer time. Generally, a single solvent gives smooth fibers [45], but mixtures of solvents give fibers with porous surfaces, especially when the difference in boiling points is large [84]. However, some research groups used a mixture of solvents (e.g. DMAc and acetone) and they got smooth fibers [63]. The porosity of fibers is an advantage, especially in nanofiber membranes, because it will increase the surface area.

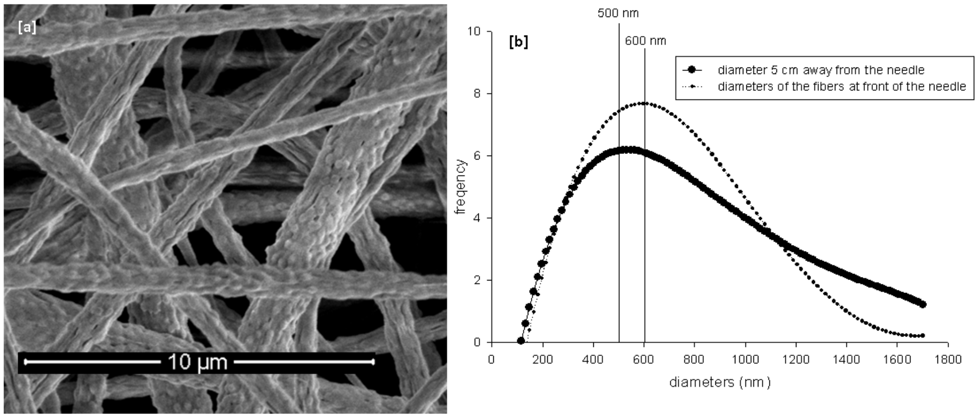

Figure 4.5. SEM micrograph of PVDF shows pores and surface roughness, [b] distribution of fiber diameters of PVDF film

Figure 4.5(b) shows the relation between the distribution of fiber diameters and the collected fibers' location (regarding the needle position). It shows that the average diameters of the fibers at the front of the needle is 600 nm, while the average diameters of the fibers that were 5 cm away from the needle position is 500 nm, which means that the collected fibers further away from the needle position will be thinner, which is due to the fibers having enough time to elongate, and the solvent to evaporate [63].

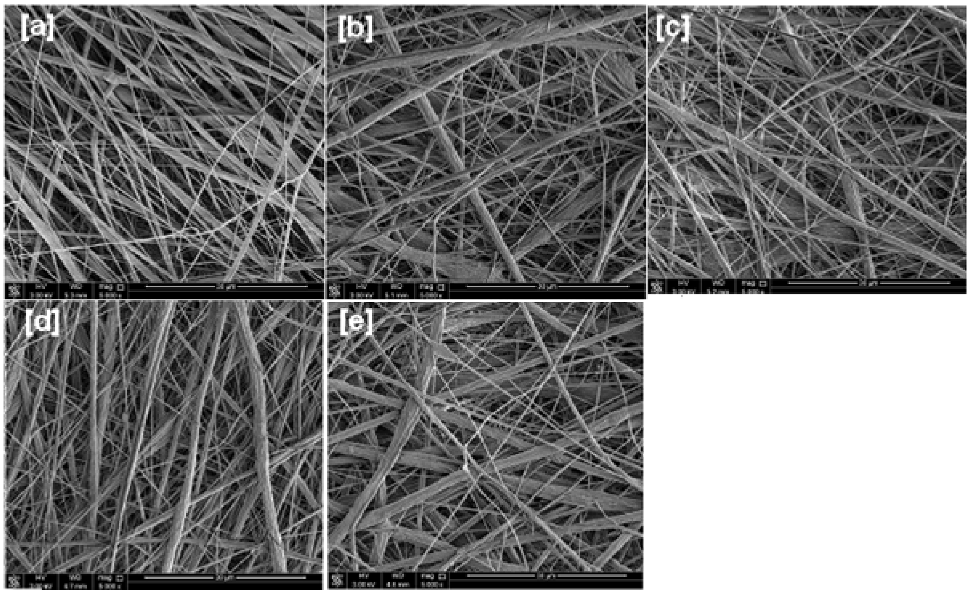

Figure 4.6. SEM micrographs of PVDF/GO composites, [a] pure PVDF, [b] 0.1 % PVDF/GO, [c] 0.3 % PVDF/GO, [d] 0.5 % PVDF/GO, [e] 0.7 % PVDF/GO

Figure 4.6 shows selected SEM micrographs of PVDF/GO nanofibrous films. It shows that nanofibers with diameters between 200 and 1700 nm were formed. The thin fibers are smoother than the thick ones due to the evaporation rate of the solvent. The nanofibers' morphology did not change noticeably with increasing the concentration of GO. Although graphene is a good conductor, GO is an insulator due to the presence of functional groups containing oxygen on the surface of the exfoliated GO layers, which causes the water molecules to be trapped between the layers. The addition of GO to a PVDF solution will therefore not increase the conductivity of the solution. Hence, the morphology of the nanofibers will be controlled by the processing parameters [22].

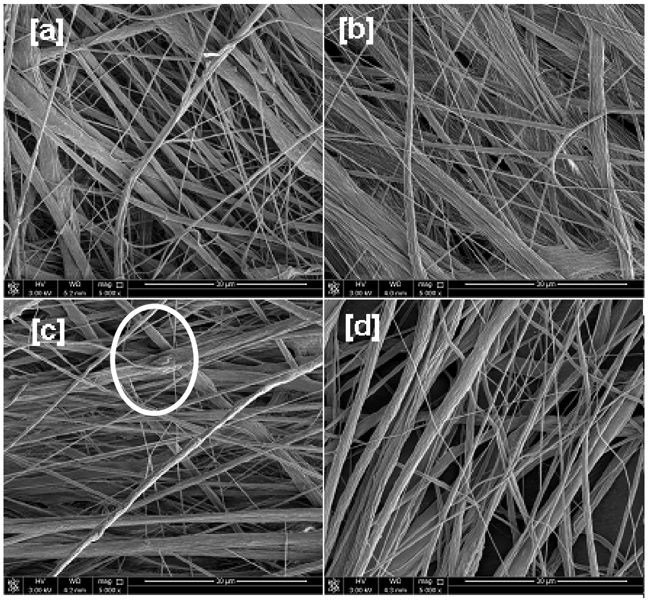

Figure 4.7 selected SEM micrographs of [a] 0 %, [b] 0.5%, [c] 1 %, and 2 %PVDF/cellulose.

The SEM micrographs of the PVDF/cellulose nanofibers do not show any noticeable improvement in the morphology (Figure 4.7). They also show that there are still some cellulose particles that deform the morphology of the fibers. It is therefore not preferred to use micro-sized cellulose fibers or particles if smooth and uniform fibers are required; cellulose nanofibers can be the solution.

Because the silver is a very good conductor, the conductivity of the PVDF/Ag-NPs solution increases with the addition of the Ag-NPs, and therefore the applied voltage of the electrospinning process should be decreased to avoid sparks.

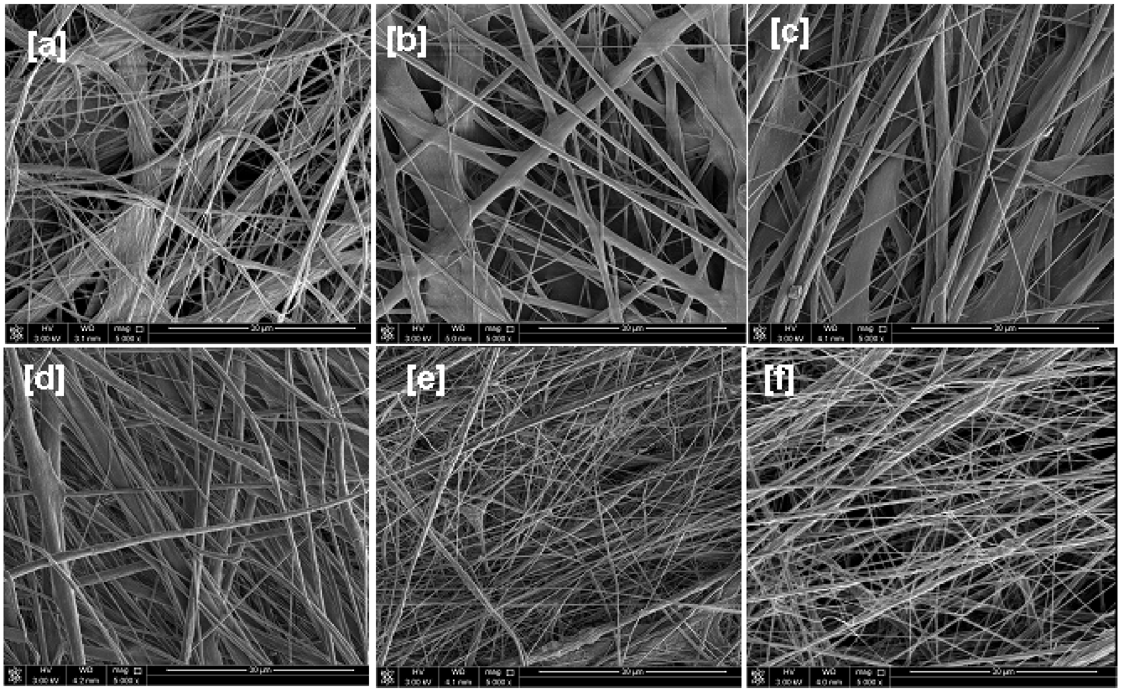

Figure 4.8. SEM micrographs of PVDF/Ag-NPs composites with different concentrations

Figure 4.8 shows selected SEM micrographs of PVDF/Ag-NPs nanofibrous fibres. Figures 4.8(a, b, c) show flat nanofibers formed beside the regular nanofibers at concentrations of 0.01, 0.02, and 0.03 % of Ag-NPs respectively. The diameters of these fibers range between 150 to 1900 nm. Figures 4.8(d, e, f) show well-defined nanofibers with thinner diameters with increasing the concentration of Ag-NPs. There is a noticeable change in the morphology of the produced fibers with the addition of Ag-NPs, starting from a concentration of 0.04% Ag-NPs. Figures 4.8(d, e, f) show that the diameters of the fibers range between 100 to 400 nm for the concentrations 0.04, 1.4, and 4.4 % of Ag-NPs respectively, in addition to a few large fibers in all the samples. The fibers became thinner and smoother with increasing concentration of Ag-NPs.

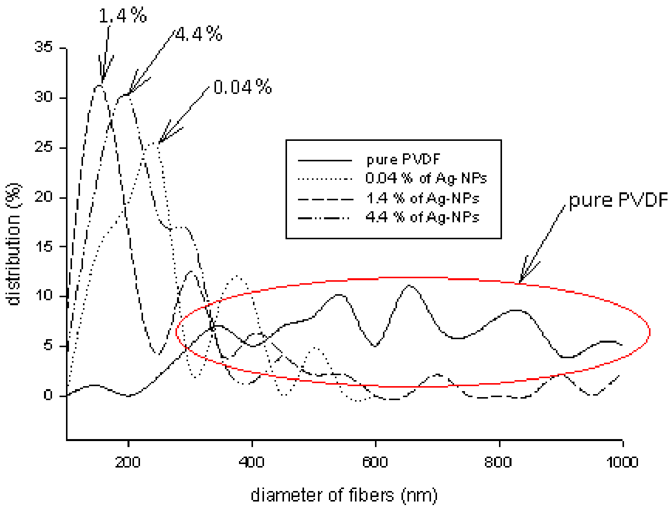

Figure 4.9. Relationship between the concentration of Ag-NPs and the distribution of fiber diameters

Figure 4.9 shows the relation between the diameters of the produced PVDF/Ag-NPs fibers and the diameters distribution with Ag-NPs concentrations. It is clear that the fibres become thinner with increasing the Ag-NPs concentration, and it tends to be more mono-disperse with increasing the concentration of the silver nanoparticles, until a certain limit (at concentration 1.4% of Ag-NPs), after which it becomes thicker and more polydisperse with increasing the concentration of Ag-NPs. It can be due to the increase in electrical and thermal conductivity of the electrospinning solution. Increasing the electrical conductivity leads to an increase in the instability elongation step in the electrospinning process and thus to the production of thin fibers [45]. In addition, the increase in thermal conductivity induces the evaporation of the two solvents (DMF and acetone) at about the same time, which leads to smoother fibers. Some researchers reported increases in thermal conductivity after the addition of silver nanoparticles [42]. However, above a certain concentration of Ag-NPs, the nanoparticles agglomerate and this leads to thicker and more poly-disperse fibers. Despite this, the addition 1.4 % of Ag-NPs with any concentration was found to lead to an improvement in the fiber morphology. Other researchers, who used silver nitrate instead of silver nanoparticles and DMF (1):acetonitrile (4) as solvent, reported that with increasing the concentration of Ag-NPs <note :- this group converted the silver nitrate to silver nanoparticles after electrospinning by using the sun light> the diameter of the produced fibers increased [85].

4.1. 3. Electrospinning samples using rotating disc collector

As discussed in Chapter 2, the rotating disk (RD), where the fibers are forced to be aligned due to the small width of the collector (3 mm), can be used as another collector to produce aligned nanofibers from (GO, cellulose, or Ag-NPs)/PVDF composites.

Figure 4.10(a) is a selected image of electrospun PVDF film. It shows the thick fibers are well aligned, but the thin fibers are not, probably due to the fact that the thin fibers are produced by more elongation in the instability step (more bending) of electrospinning process, and then they deposit on the rotating disk more freely. In addition, there are flat fibers with rough surfaces. Figure 4.10(b) shows the distribution of the fiber diameters, which range between 150 to 2000 nm, with most of the fibers lying between 200 and 650 nm with a peak value at 320 nm. Even though the thick fibers in the SEM photo seem to be dominating, the distribution curve shows that the thinner ones dominate.

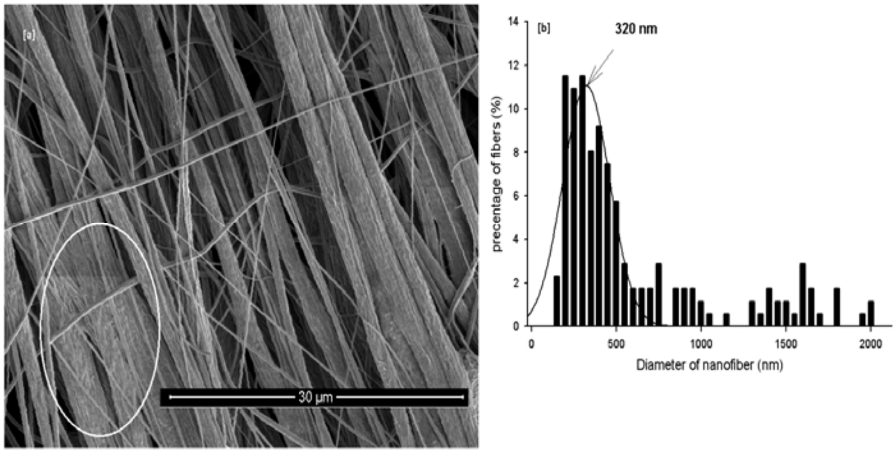

FIGURE 4.10. [A] SEM MICROGRAPH, [B] FIBER DIAMETER DISTRIBUTION CURVE OF ELECTROSPUN PVDF FILM BY ROTATING DISK

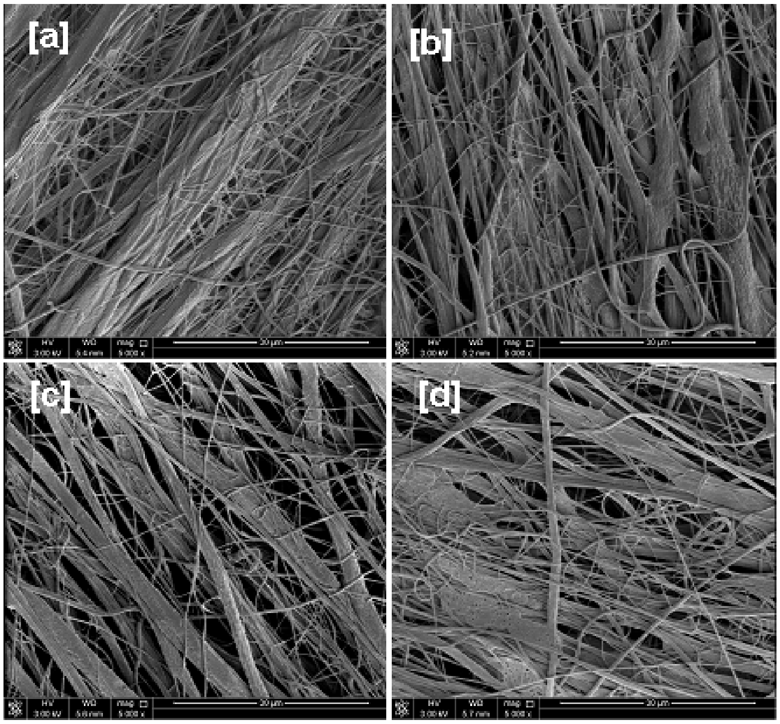

Figure 4.11. SEM micrographs of PVDF/GO composites with different concentrations [a] 0.1 %, [b] 0.3 %, [c] 0.5 %, and [d] 0.7 % with rotating disk

Figure 4.11 shows selected SEM images of the PVDF/GO composites. The micrographs show that the fibres are aligned but fused together, and a higher applied voltage (11.5 kV) will not have made any difference. The reason could be that the GO is not conductive, and the applied voltage should be increased more, or the DMF is a good solvent for GO and hence adding more GO leads to the stabilization of PVDF solution in DMF, and therefore cannot be dry easily [86]. < note ,Because the acetone evaporated immediately and leave the DMF due to the high boiling of the DMF and the surface area of collator is very small.>

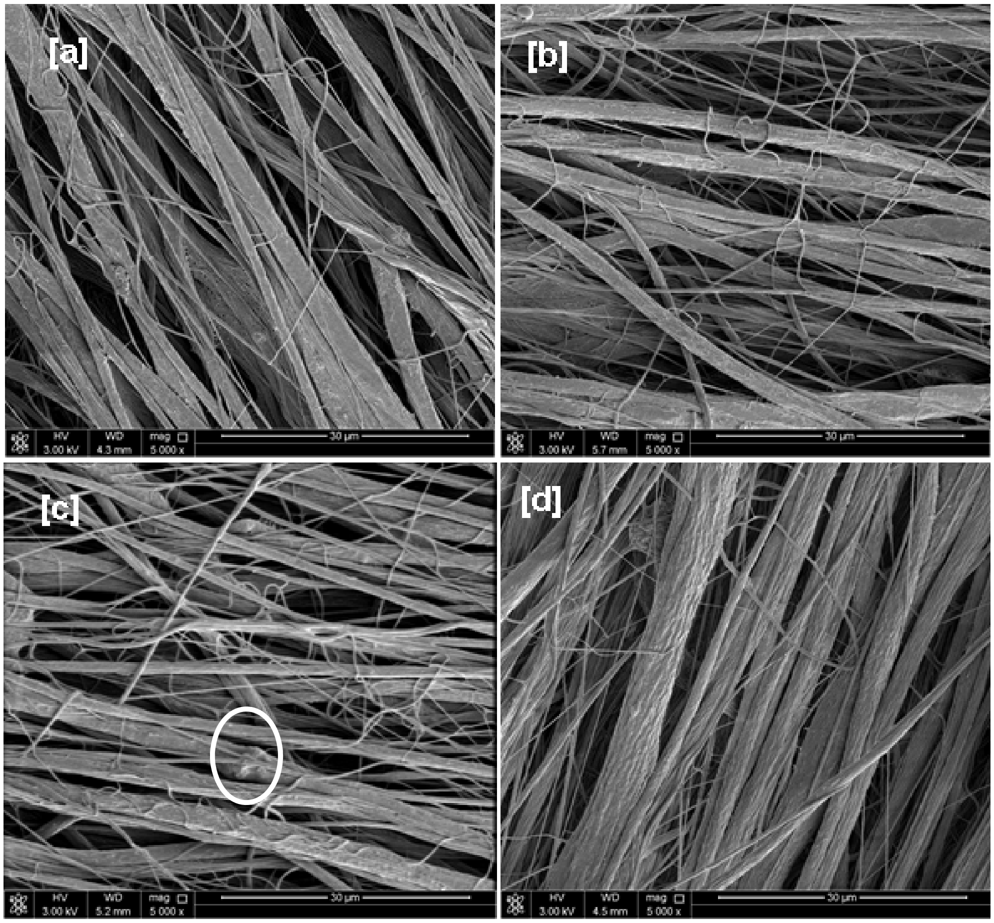

Figure 4.12. SEM micrographs of [a] 0.5%, [b] 1.0%, [c] 2.0% %, [d] 4% PVDF/cellulose with rotating disk. The circle shows the deformation of the fiber

Figure 4.12 shows selected SEM images of PVDF/cellulose composites. It shows that the fibers are aligned and that they become more cylindrical with increasing the concentration of the cellulose. The diameters of the produced nanofibers decreased with increasing the concentration of cellulose. The enhancement of the fiber morphology could be due to the absorption of the solvents (specially the DMF) by the cellulose fibers, which led to well-defined fibers. The swelling power of the cellulose to DMF and acetone are 62 and less than 15 (g/g), respectively [87]. <note:- the aggregation affect the crystallinity and beta phase not the morphology, where the morphology depends on the conductivity of the solution or as in this case the swelling power of the cellulose, in there are some deformation due to the size of cellulose particles>

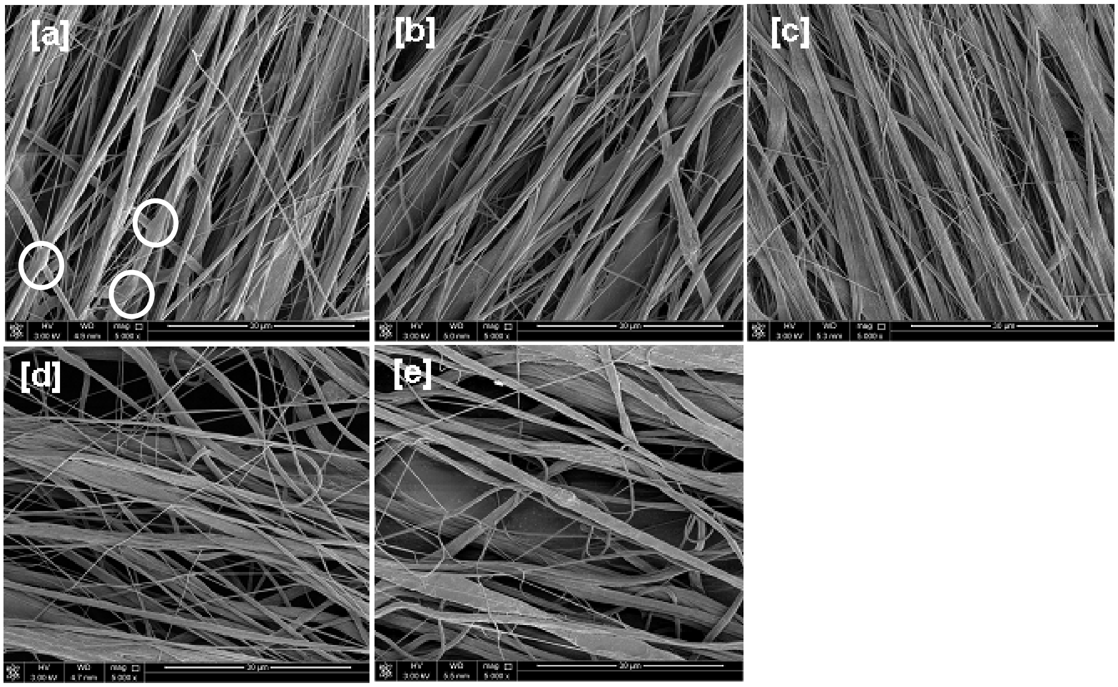

Figure 4.13. SEM micrographs of PVDF/Ag-NPs of concentration [a] 0.2 %, [b] 0.4 %, [c] 0.6 %,[d] 0.8%, and 1.0 %; the circles show the fibers are still soft.

Figure 4.13(a-c) show selected SEM images of PVDF/Ag-NPs with concentrations 0.2, 0.4, and 0.6 % respectively. They show that the fibers were not completely dry when deposited on the rotating disk collector. The fiber diameters ranged from 230 to 1700 nm, and these diameters decreased with increasing the concentration of Ag-NPs. The fibers are also highly aligned. However, Figure 4.13(d,f) show that there are more of the thinner fibers than the thicker ones, especially in 0.8% concentration of PVDF/Ag-NPs, and the fibers are less aligned. The reason could be the increase in the conductivity of the PVDF/Ag-NPs solutions which led to an increase in the instability of the elongation step in the electrospinning process.

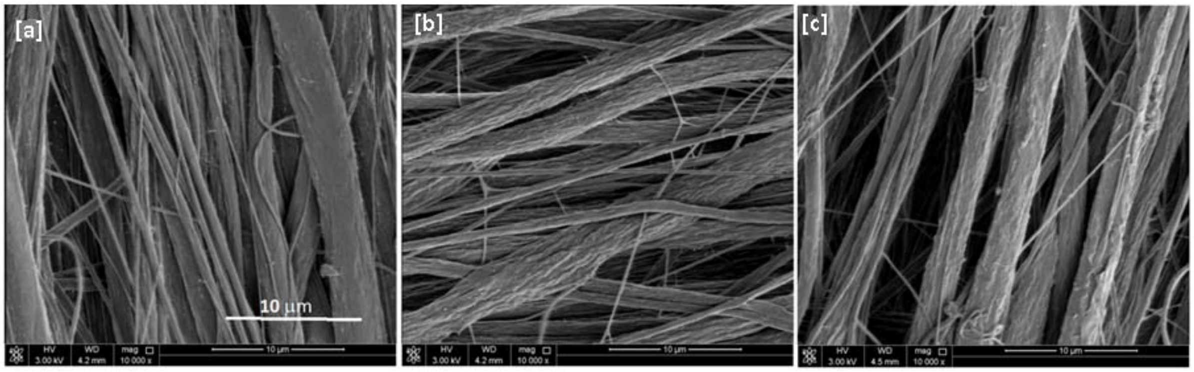

Figure 4.14. SEM micrograph of [a] M1, [b] M2, and [c] M3

Figure 4.14(a) is a SEM micrograph of a mixture (M1) which contained 0.4% of Ag-NPs and 0.3% of GO. It shows aligned small cylindrical fibers and flat wide fibers. It is clearly shows the effect of both fillers, with the thin and cylindrical fibers resulting from the silver particles, and the flat wide fibers from the GO sheets. Figure 4.14(b) is a SEM micrograph of a mixture (M2) which contained 0.4% of Ag-NPs with 1% of cellulose. It shows thick, aligned fibers with a small number of thinner fibers. The thick fibers are rough as in the case of the fibers of the PVDF/cellulose composites, and the thinner fibres are smooth. Figure 4.14(c) is a SEM micrograph of a mixture (M3) which contained 0.4% of Ag-NPs, 0.3% of GO, and 1% of cellulose. It shows thick fibers with very few thin fibers.

Figure 4.15 (a, d) are a SEM micrograph and fiber diameter distribution curve of PVDF, and it shows the formation of nanofibers as explained before. Figure 4.15(b, e) are the SEM photo and fiber diameter distribution curve of 0.5% PVDF/TEAC respectively. It shows that the fibers become thinner, and tend to be mono-disperse when compared to those of pure PVDF. The average diameter is 220 nm, and most of the fibers have diameters less than 500 nm. Figure 4.15(c, f) are the SEM photo and fiber diameter distribution curve of NaCl/PVDF nanofibers. It shows that most of fibers have diameters less than 500 nm, and the average diameter is 250 nm, although some thick fibers are observed. The improvement in the diameter thickness is due to the increase in the conductivity of the electrospinning solution with addition of the salts; the improvement in the case of TEAC is more than that in the case of NaCl due to the TEAC being soluble in the organic solvent, while NaCl is not [65, 66]. < note :- yours are right but I focus on the filler>

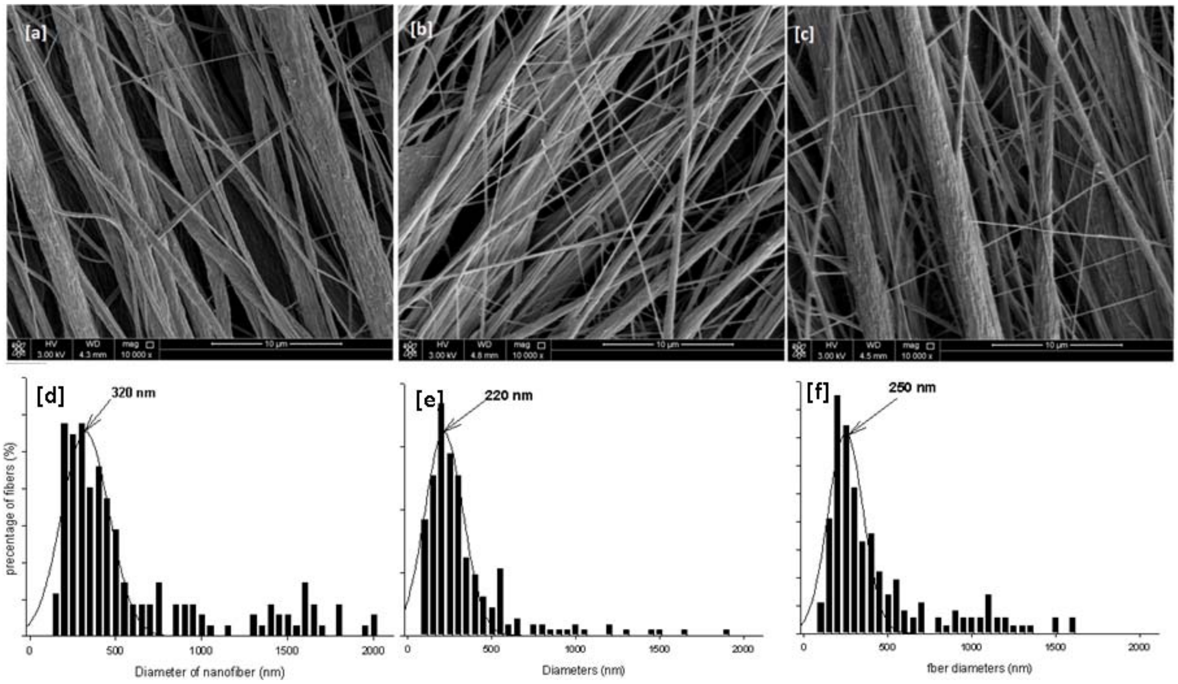

Figure 4.15. SEM micrograph of [a] PVDF, [b] TEAC/PVDF, and [c] NaCl/PVDF, and fiber diameter distribution curves of [d] PVDF, [e] PVDF/TEAC, and [f] PVDF/NaCl

4. 2. Crystallinity and β-phase content

4.2. 1. Crystallinity (by DSC)

Most of the articles refer to the DSC technique as a complementary technique for FTIR and XRD in the identification of PVDF phases, because it does not depend on the PVDF phases only, but also on the crystal defects, which is affected by the processing conditions and filler additives. Where the melting point of the β- and α-phases are between 167 and 172 °C, the γ-phase is between 179 and 180 °C, and the γ’-phase between 189 and 190 °C [2]. These values change with polymer molecular weight; in the case of PVDF with an average molecular weight (250000 amu), the melting point varies between 156.3 to 160.3, depending on the processing parameters [65].

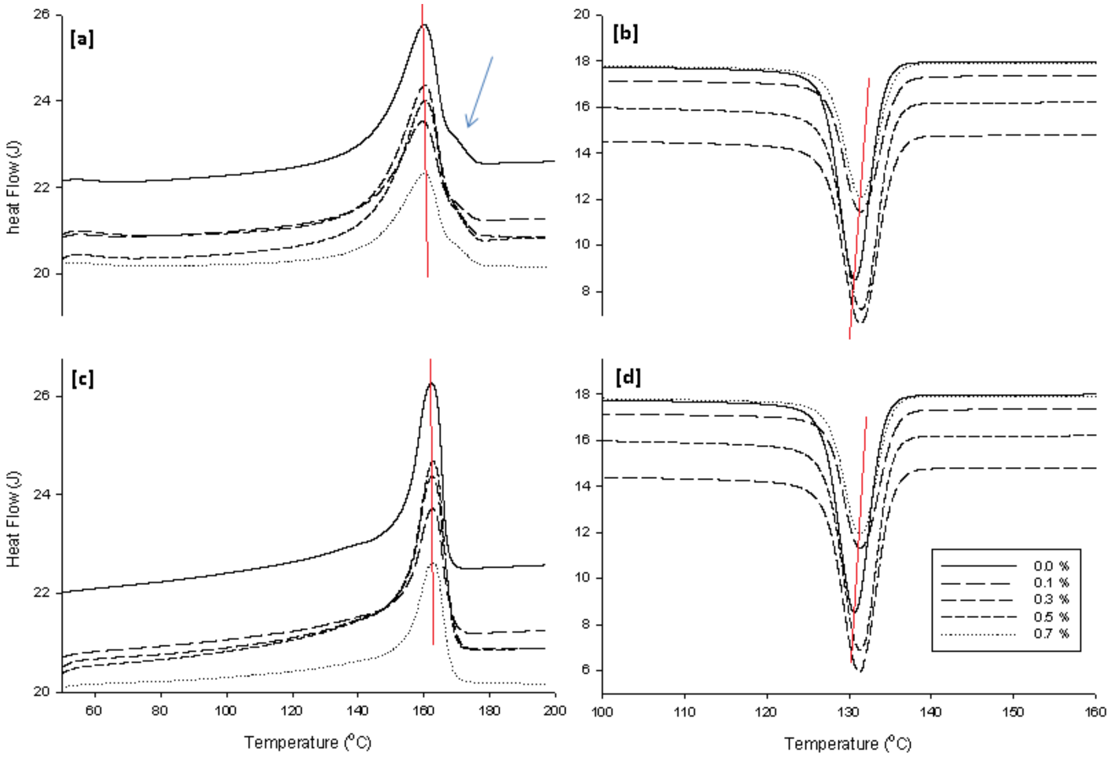

Figure 4.16. DSC thermograms of electrospun PVDF/GO films. [a] first heating cycle, [b] first cooling cycle, [c] second heating cycle, [b] second cooling cycle

Figure 4.16 shows the thermograms of PVDF and of PVDF/GO composites, and the effect of the of GO loading. Figure 4.16(a, c) show the first and second heating cycle, and the melting temperature (T_m) of first and second heating cycles of the samples around 160 and 162.4 °C respectively, without any significant effect of GO concentration. Figure 4.16(b, d) shows the first and second cooling cycles, and the crystallization temperatures (T_c) from the first and second cooling are identical for each concentration. A slight increase with increasing the concentration of GO is noticed. The difference between the first and second melting points is due to differences in the crystal sizes. The first heating is of the melt-spun fiber in which only small crystals formed because of the fast solvent evaporation, while the second heating shows the melting of crystals formed during controlled cooling and therefore had enough time to grow [76]. Figure 4.16(a).

shows that there is another phase at 170 °C, which could be the γ-phase, because the α- and β-phases appear at the same temperature which is 8 °C lower than that of the γ-phase [2]. However, some articles attribute this peak to the beta phase [16]. <note :- the peak at 170 °C is disappeared due to the phases of the PVDF are converted to α-phase after first melting.>

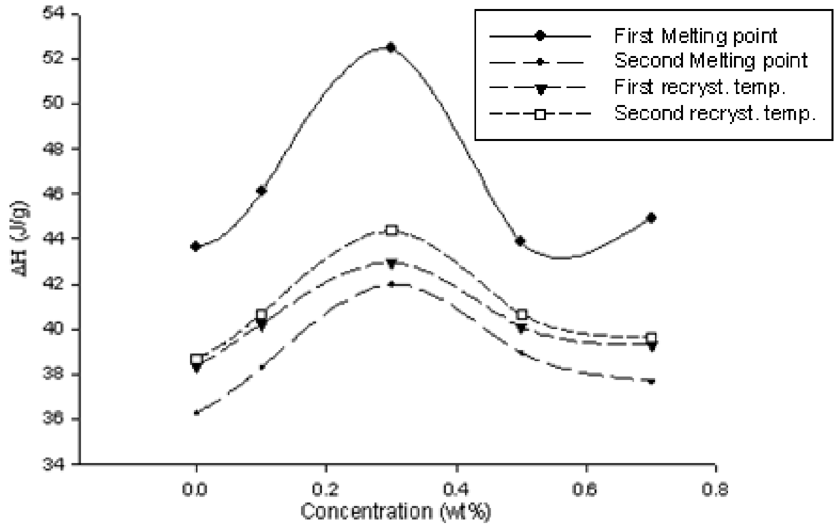

Figure 4.17. the relationship between the concentration of GO and the enthalpies (ΔH) of GO films at different melting and crystallization points (phase change)

Figure 4.17 shows the relation between the enthalpies of PVDF/GO composites at different concentrations. The enthalpy values of all the samples increase to a maximum at a GO concentration of 0.3%, and then decrease. This improvement can be explained as the (i) GO sheets (see Figure 4.1) acting as nucleating agents by providing a large surface area to crystallize PVDF from the solution [73]; and/or (ii) the formation of a beta phase which is a more compact phase than the α-phase, and which needs more energy to melt than the α-phase [16]. Then the enthalpies decreases due to agglomeration of the GO sheets.

It is noticed in Figure 4.17 that the difference between the first and second heating cycles is almost the same, which is due to the effect of the processing history, but at 0.3% the difference is bigger, which is due to the presence of the β-phase which was confirmed by XRD and FTIR measurements. The degree of crystallinity was calculated by using equation (4), where ΔH_o equals 104.6 J/g. Table 4.1 shows that the crystallinities were higher than the value (35%) reported in literature [16], and even higher with increasing GO concentration.

Table 4.1. The enthalpies (ΔH) and degree of crystallinity of PVDF/GO

C	ΔH_{m1}	X_{c1}	ΔH_{m2}	X_{c2}	ΔH_{c1}	X_{c3}	ΔH_{c2}	X_{c4}
0 %	43.7	41.7	36.3	34.7	38.3	36.7	38.7	37.0
0.1 %	46.1	44.1	38.3	36.6	40.2	38.5	40.7	38.9
0.3 %	52.5	50.2	42.0	40.2	43.0	41.1	44.4	42.4
0.5 %	43.9	41.9	38.9	37.2	40.	38.3	40.6	38.9
0.7 %	44.9	43.0	37.7	36.0	39.3	37.6	39.6	37.9

C is the concentration of GO, ΔH_{m1} and ΔH_{m2} are the melting enthalpies (J/g) of the first and second cycles respectively, ΔH_{c1} and ΔH_{c2}, are the crystallization enthalpies (J/g) of the first and second cycles respectively, X_{c1}, X_{c2}, X_{c3}, and X_{c4} are the degrees of crystallinity (%) for the GO composites at the first and second heating cycles, and the first second cooling cycles respectively

Figure 4.18 shows the thermograms of the PVDF samples and the PVDF/cellulose composites, and the effect of the amount of cellulose in the composites. Figure 4.18(a, c) shows that the melting points of the first heating cycle are identical (around 160 °C) regardless of the concentration of the cellulose, and the same behavior was observed for the second heating cycle (around 162 °C). There is a difference of 2.1 °C between the melting temperatures in the first and second heating cycles. The first and the second crystallization temperatures of each concentration are identical, and cellulose addition increased the crystallization temperatures (Figure 4.18(b, c)). Figure 4.18(a) shows that the prepared films contain more than one crystalline structure.

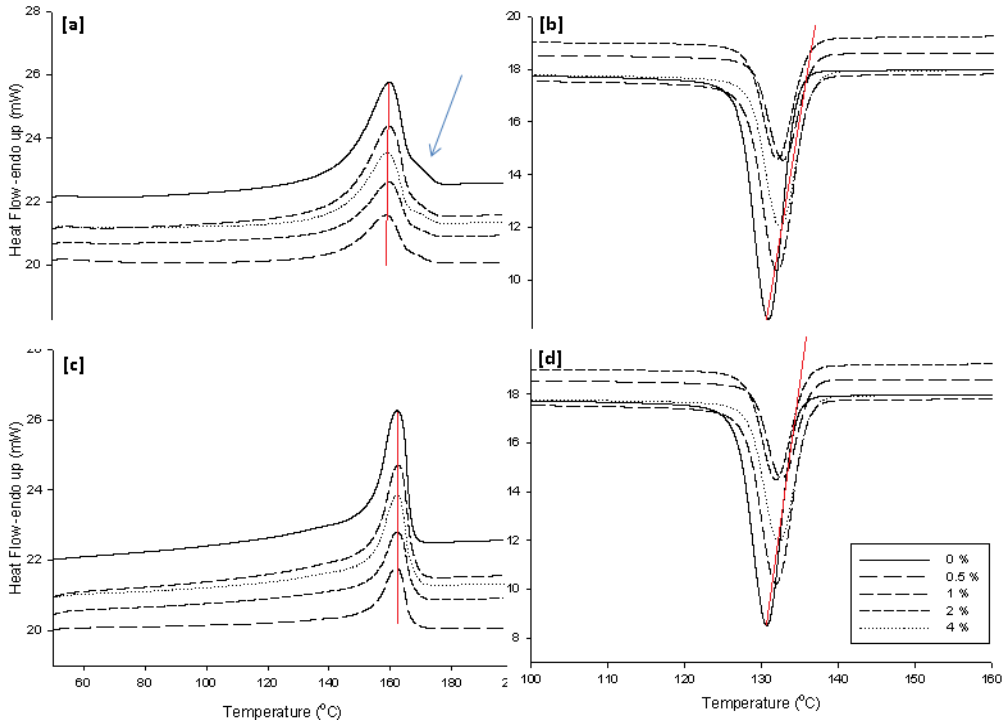

Figure 4.18. DSC thermograms of electrospun PVDF/cellulose films. [a] first heating cycle, [b] first cooling cycle, [c] second heating cycle, [b] second cooling cycle

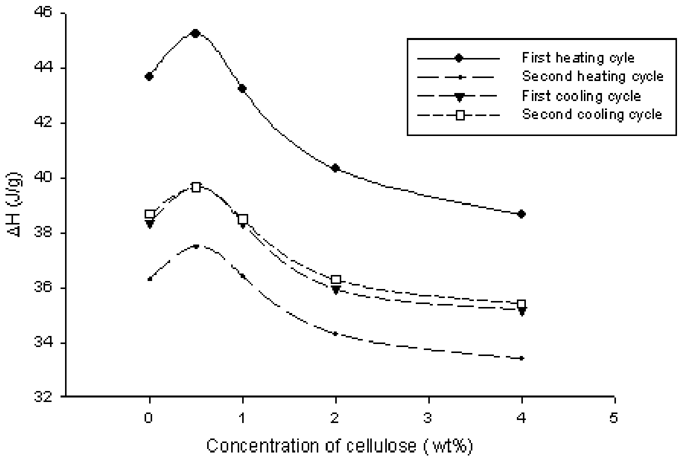

Figure 4.19. The relationship between the concentration of cellulose and the enthalpies (ΔH) of cellulose films at different melting and crystallization points (phase change)

Figure 4.19 shows a relation between the enthalpies and the concentration of PVDF/cellulose at different heating and cooling cycles. It shows that the enthalpy value depends on the concentration of the cellulose, and a maximum value was observed at a concentration of 0.5 %. The difference between the first and second heating cycle curves are also equal (6 J/g) regardless of the concentration of cellulose.

Table 4.2 shows that the maximum degree of crystallinity (43.2%) is obtained at 0.5% concentration of cellulose. Addition of cellulose caused a decrease in the crystallinity values to a value below that of pure PVDF. Rajesh et al. [5] found that the crystallinity of PVDF cellulose films which was prepared by casting from different types of cellulose, decreased with increasing the concentration of most cellulose types. The same group found that the crystallinity of PVDF and a cellulose nano-whiskers composite first increased to a concentration of 0.5 % of cellulose, and then decreased, which is similar to our own observations. < note :- I used a commercial cellulose with different dimensions but in general, it is smaller than what this group used , so I think the small particles of the cellulose lead to improvement at the beginning, and then the aggregation due to hydrophobicity of the PVDF lead to formation of isolated islands of cellulose inside the PVDF lead to decrease the crystallinity.>

We observed a higher crystallinity for pure PVDF than the 30.5% reported by Rajesh et al., which indicate that the processing technique enhanced the crystallinity, because they used PVDF with molecular weight equal to the one we used.

Table 4.2. The enthalpies (ΔH) and degree of crystallinity of PVDF/cellulose

C	ΔH_{m1}	X_{c1}	ΔH_{m2}	X_{c2}	ΔH_{c1}	X_{c3}	ΔH_{c2}	X_{c4}
0	43.7	41.7	36.3	34.7	38.3	36.7	38.7	37.0
0.5	45.2	43.2	37.5	35.8	39.7	37.9	39.6	37.9
1	43.2	41.3	36.4	34.8	38.4	36.7	38.5	36.8
2	40.3	38.5	34.3	32.8	35.9	34.3	36.3	34.7
4	38.6	36.9	33.4	31.9	35.2	33.6	35.4	33.8

C is the concentration of cellulose, ΔH_{m1} and ΔH_{m2} are the melting enthalpies (J/g) of the first and second cycles respectively, ΔH_{c1} and ΔH_{c2}, are the crystallization enthalpies (J/g) of the first and second cycles respectively, X_{c1}, X_{c2}, X_{c3}, and X_{c4} are the degrees of crystallinity (%) for the GO composites at the first and second heating cycles, and the first second cooling cycles respectively

Figure 4.20 shows the thermograms of the heating and cooling cycles of PVDF/Ag-NPs composites. The melting and crystallization temperatures are identical to those of the PVDF/GO and PVDF/cellulose composites, which mean that the phase change temperature does not depend on the filler nature, but on the size of the PVDF crystals, which depends on the concentration of the filler.

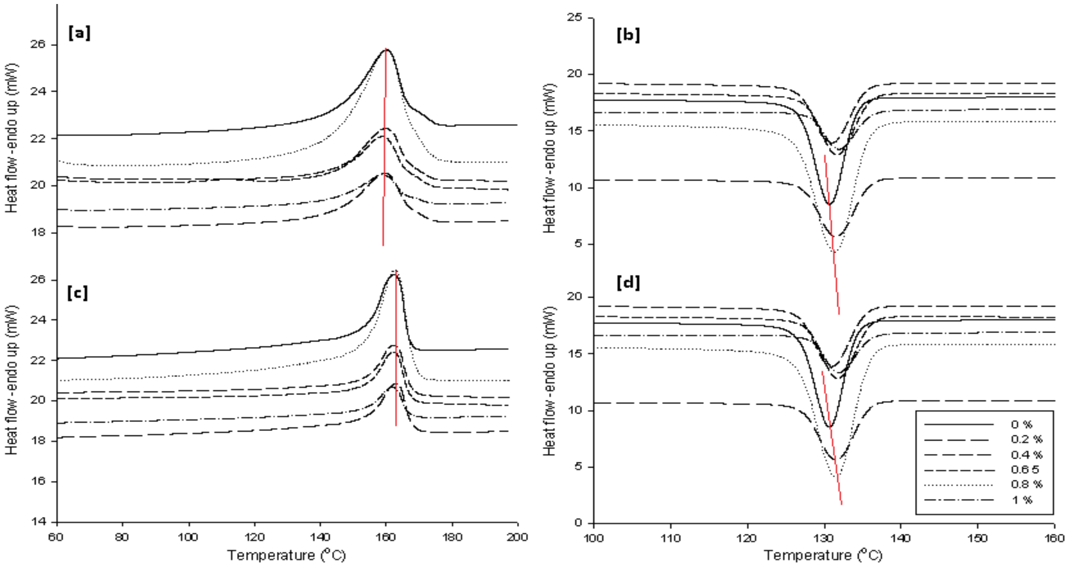

Figure 4.20. DSC thermograms of electrospun PVDF/Ag-NPs films. [a] first heating cycle, [b] first cooling cycle, [c] second heating cycle, [b] second cooling cycle

Figure 4.21 shows the relation between the enthalpies of PVDF/Ag-NPS and the Ag-NPs concentration. It shows that the enthalpy values increase with increasing Ag-NPs content, with the highest enthalpy at a concentration 0.4% of Ag-NPs. The difference between the enthalpies of first and second heat cycles are constant and equal to 8 J/g, and the increase in crystallization is due to using the Ag-NPs as nucleating agent.

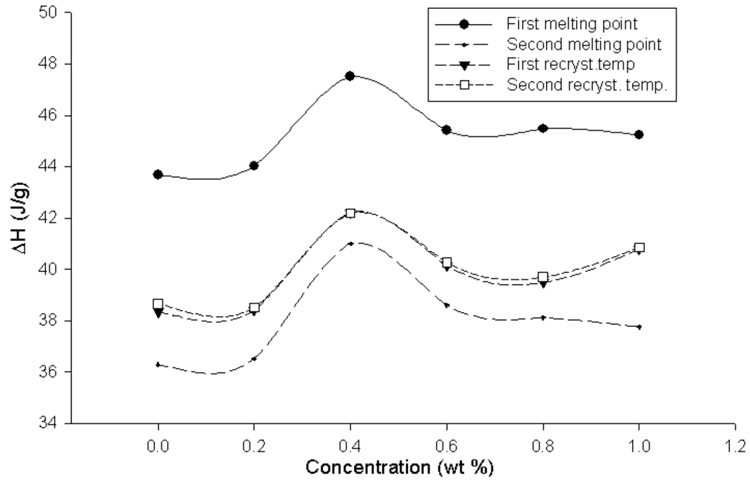

Figure 4.21. The relationship between the concentration of Ag-NPs and the enthalpies (ΔH) of Ag-NPs/PVDF films at different melting and crystallization points (phase change)

Table 4.3. The enthalpies (ΔH) and degree of crystallinity of PVDF/Ag-NPs

C	ΔH_{m1}	X_{c1}	ΔH_{m2}	X_{c2}	ΔH_{c1}	X_{c3}	ΔH_{c2}	X_{c4}
0	43.7	41.7	36.3	34.7	38.3	36.7	38.7	37.0
0.2	44.0	42.1	36.5	34.9	38.4	36.7	38.5	36.8
0.4	47.	45.4	41.0	39.2	42.2	40.4	42.2	40.3
0.6	45.4	43.4	38.6	36.9	40.1	38.4	40.3	38.5
0.8	45.5	43.5	38.1	36.4	39.5	37.8	397	38.0
1	45.2	43.2	37.8	36.1	40.8	39.0	40.9	39.1

C is the concentration of Ag-NPs, ΔH_{m1} and ΔH_{m2} are the melting enthalpies (J/g) of the first and second cycles respectively, ΔH_{c1} and ΔH_{c2}, are the crystallization enthalpies (J/g) of the first and second cycles respectively, X_{c1}, X_{c2}, X_{c3}, and X_{c4} are the degrees of crystallinity (%) for the GO composites at the first and second heating cycles, and the first second cooling cycles respectively

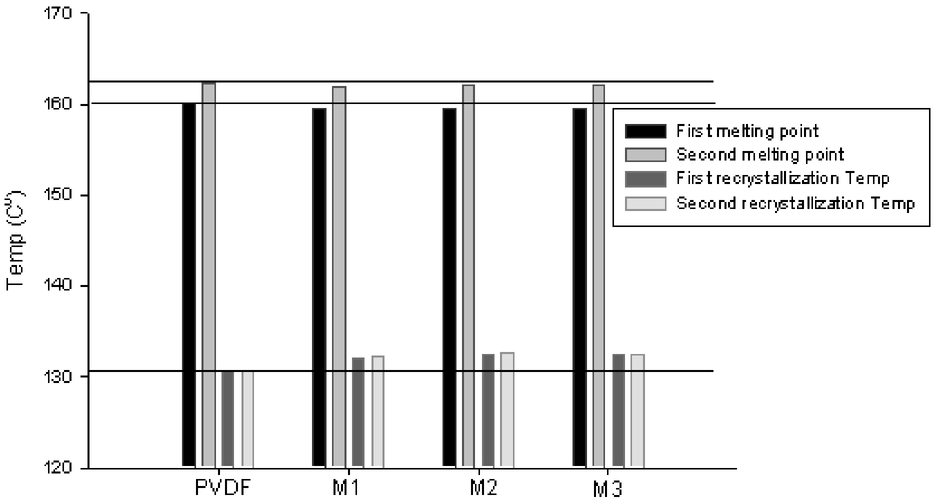

Figure 4.22. The melting and crystallization temperatures of PVDF and the mixtures

Table 4.4. The enthalpies (ΔH) and degree of crystallinity of the mixtures

C	ΔH_{m1}	X_{c1}	ΔH_{m2}	X_{c2}	ΔH_{c1}	X_{c3}	ΔH_{c2}	X_{c4}
PVDF	43.7	41.7	36.3	34.7	38.3	36.7	38.7	37.0
M1	42.8	40.9	36.8	35.2	38.3	36.6	38.3	36.6
M2	43.9	42.0	37.6	35.9	39.8	38.0	39.9	38.1
M3	45.4	43.4	38.7	37.0	40.6	38.8	40.9	39.1
0.4 (Ag)	47.5	45.4	41.0	39.2	42.2	40.4	42.2	40.3
0.3 (Go)	52.5	50.2	42.0	40.2	43.0	41.1	44.4	42.4
1 % (cell)	43.2	41.3	36.4	34.8	38.4	36.7	38.5	36.8

C is the code of the samples, ΔH_{m1} and ΔH_{m2} are the melting enthalpies (J/g) of the first and second cycles respectively, ΔH_{c1} and ΔH_{c2}, are the crystallization enthalpies (J/g) of the first and second cycles respectively, X_{c1}, X_{c2}, X_{c3}, and X_{c4} are the degrees of crystallinity (%) for the GO composites at the first and second heating cycles, and the first second cooling cycles respectively, (cell) means PVDF/cellulose composite

Figure 4.22 shows the melting and crystallization temperatures of PVDF and mixtures from selected ratios of the fillers (Ag-NPS, cellulose, and GO), as defined in the materials and methodology chapter. The figure shows that the melting points of the mixtures are slightly lower than that of pure PVDF for the two cycles. In addition it shows that the crystallization temperatures (T_c) are higher than that of the PVDF in the two cooling cycles, as expected due to the effect of the fillers.

The degrees of crystallinity are improved from 41.7 % for PVDF to 43.4 % for M3 (Table 4.4), while the crystallinity of M1 (0.4 % of Ag-NPs and 0.3 % of GO) is lower than that of pure PVDF due to the agglomeration of GO sheets, and the aggregation of Ag-NPs. If the results of the mixtures are compared with those of the pure PVDF/filler composites, it is clear that the crystallinities of the mixtures are lower than those of all the pure composites. This is probably due to the hetero-nucleation effect of the different fillers.

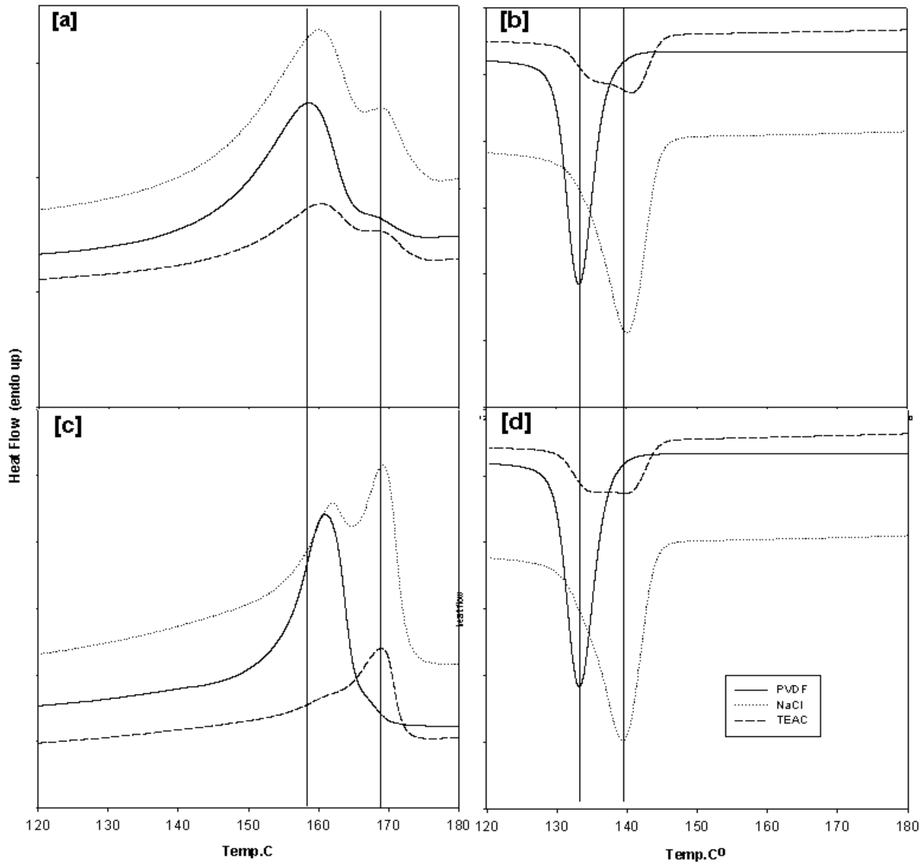

Figure 4.23. Thermograms of [a] first heating cycle, [b] first cooling cycle, [c] second heating cycle, and [d] second cooling cycle for PVDF and PVDF with salts

Figure 4.23(a, c) shows the thermograms of the heating cycles of PVDF and PVDF with salts. It shows unexpected behavior, because for the GO, cellulose, and Ag-NPs the DSC thermograms showed the dominating phases to be the beta or alpha phase with only small amounts of ϒ-phase, which changed completely to the alpha phase during cooling after the first heating cycle. In the case of the salts, however, the DSC first heating thermograms showed the presence of alpha and/or beta phases with an appreciable quantity of the gamma phase, which crystallized almost completely into a gamma phase during cooling after the first heating. Figure 4.23(b, d) confirms these observations.

Table 4.5. The enthalpies (ΔH) and degree of crystallinity of PVDF with salts

Sample	ΔH_{m1}	X_{c1}	ΔH_{m2}	X_{c2}	ΔH_{c1}	X_{c3}	ΔH_{c2}	X_{c4}
PVDF	43.7	41.7	36.3	34.7	38.3	36.7	38.7	37.0
PVDF/NaCl	48.8	46.6	48.0	45.9	47.4	45.3	48.6	46.5
PVDF/TEAC	40.8	39.0	40.4	38.7	42.2	40.4	42.3	40.5

ΔH_{m1} and ΔH_{m2} are the melting enthalpies (J/g) of the first and second cycles respectively, ΔH_{c1} and ΔH_{c2}, are the crystallization enthalpies (J/g) of the first and second cycles respectively, X_{c1}, X_{c2}, X_{c3}, and X_{c4} are the degrees of crystallinity (%) for the samples at the first and second heating cycles, and the first second cooling cycles respectively

Table 4.5 shows that the PVDF/NaCl is more crystalline than the PVDF, and the PVDF/TEAC is less crystalline than both of them. However, the degree of crystallinity for the PVDF/salt composites determined from the first and second heating and cooling cycles are almost similar.

4.2. 2. Investigation of the β-phase content in the samples (by FTIR)

Most researchers used FTIR to investigate the presence of the beta phase. However, the conformation of the beta phase is similar to that of the gamma phase, which causes some confusion because most of the beta phase bands are very close to those of the gamma phase as shown in table 4.6.

Table 4.6. Characteristic FTIR wavenumbers for each phase of PVDF. The values were obtained from ref [2, 73, 88]

	α-phase	**β-phase**	**γ-phase**
Wavenumbers (cm^{-1})	408	510	431
	532	840	512
	614	1279	776
	766	485	812
	795	440	833
	855		840
	976		1234

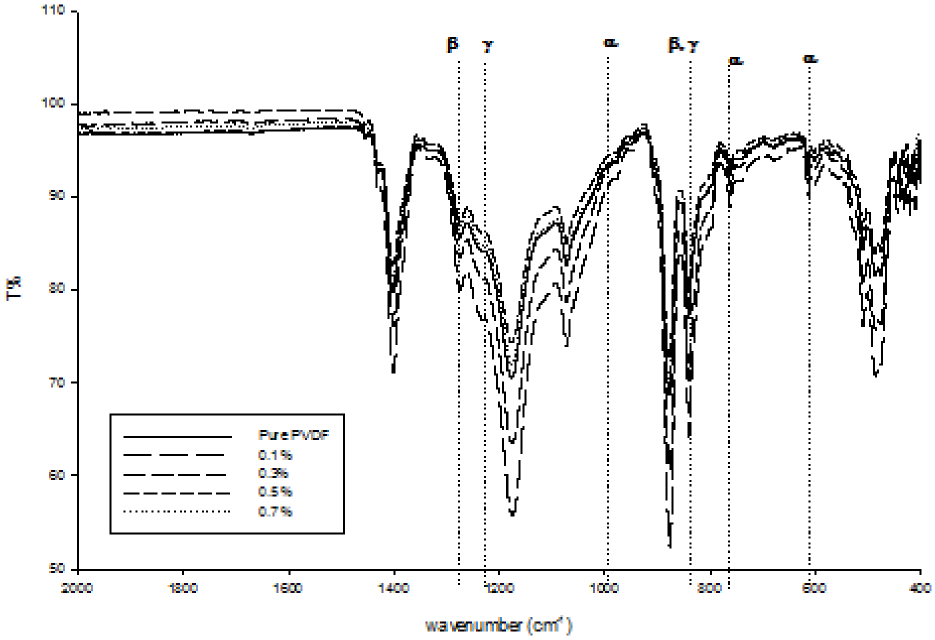

Figure 4.24. FTIR spectra of PVDF/GO composites

Figure 2.24 shows the presence of the β- and α-phases, and also a weak gamma phase peak at 1234 cm^{-1}. Equation (7) is used to calculate the percentage of beta phase in the PVDF/GO samples, and the results are shown in Figure 4.25, which shows the relation between the concentration of GO and the β-content percentage. The β-content has a maximum value at a concentration of 0.1% after which it decreased with an increase in the GO concentration. This is due to the presence of oxygen in GO as a carboxylic group (>C=O) which reacts with the >CF_2 group and leads to a decrease in the energy of the α-phase, hence it converts to the β-phase [36].

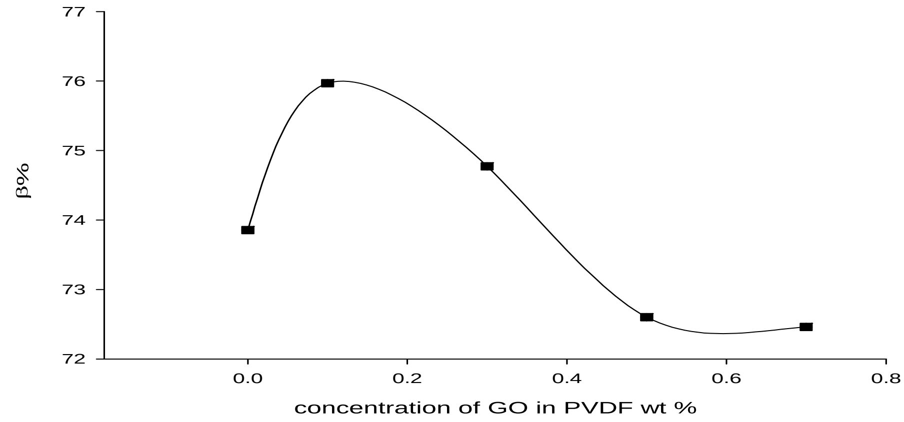

Figure 4.25. Beta content in PVDF/GO composites

The same result was obtained by the Achaby group [36], who found that at 0.1%of GO the only available phase is the β-phase, and the same phase content was observed even with increasing the GO percentage. The difference between our results may be due to (i) the fabrication technique, because they used casting, and we used electrospinning, (ii) solvent, because they used DMF only and we used DMF/acetone, and DMF is known as a good solvent for GO, and (iii) they used ultrasonication to disperse the GO while we only used a magnetic stirrer.

Figure 4.26 shows the relation between the calculated beta phase content and the concentration of cellulose. The beta phase content increased as the concentration of cellulose increased up to a maximum of 80% at 1.0% cellulose, after which the β-content decreased with increasing the concentration of cellulose. A maximum β-phase content (about 82%) was obtained at a concentration of 1% cellulose by another group [15]; they used a casting technique and uniform rod-like cellulose. The beta phase content therefore seems to depend on the concentration of cellulose regardless of the shape of the filler. The enhancement in β-phase is due to the presence of -OH groups, that are rich with oxygen atoms which interact with fluorine atoms [15].

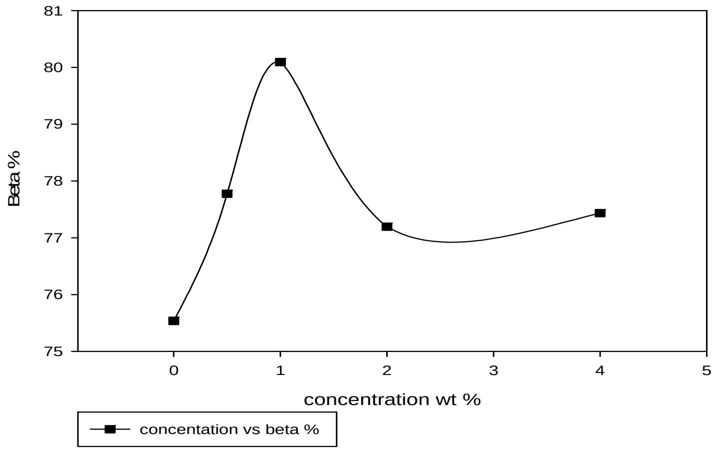

Figure 4.26. Beta content in PVDF/cellulose composites

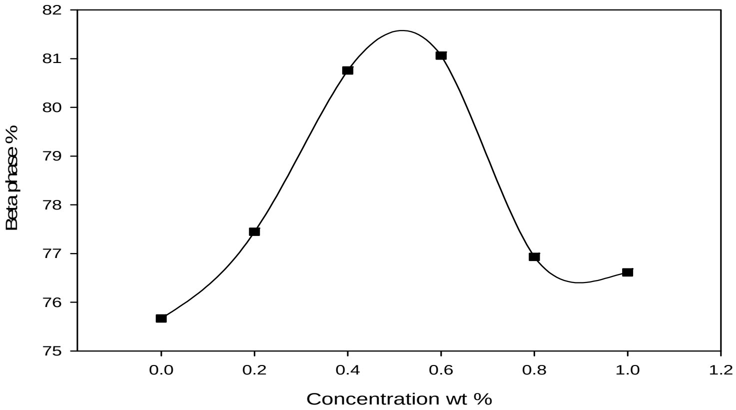

Figure 4.27. Beta content at PVDF/Ag-NPs composites

Figure 4.27 shows that the beta content increased with increasing the concentration of Ag-NPs with a maximum at 0.5% Ag-NPs, and then decreased again with increasing the Ag-NPs percentage. The enhancement in the β-phase was due to (i) the Ag-NPs acting as nucleating agents which led to an increase in the crystallinity, (ii) the Ag-NPs surfaces that were rich with electrons, and which worked as a local dipole which attracted the fluorine atoms to form a beta phase conformation. Ag-NPs therefore improved the crystallinity and the beta phase at the same time [12, 85]. Li et al. [12] observed a maximum beta phase at a concentration of 1.5% of silver nanowires, and this difference may be due to the surface area of the nanoparticles being larger than that of the nanowires, where the beta phase formation especially depends on the local dipole which is formed on the surface of the silver nanoparticles [12]. With increasing the concentration of Ag-NPs, the particles will aggregate as seen in Figure 4.3(b). This can lead to a decrease in the local dipole surfaces. Another research group used silver nitrate to enhance the beta phase content by a casting technique, and they found that the maximum beta phase was at a filler concentration of 0.5%. The β-phase enhancement was due to the interaction between the Ag-atoms in the nitrate salt and the F-atoms in the PVDF molecule. The main rule in the developing the beta phase is the electrons on the Ag surface regardless of whether they are ions or atoms [12, 85].

Table 4.7. β-phase content in the mixtures and PVDF with salts

Sample	**PVDF**	**M1**	**M2**	**M3**	**NaCl/PVDF**	**TEAC/PVDF**
β-phase content%	75.7	76.3	83.1	80.5	86.4	79.1

Table 4.7 shows the beta content in the PVDF, the mixtures, and PVDF with the salts. The maximum value was obtained by using sodium chloride at a concentration of 0.5%, which could be due to an increase in the gamma phase content as shown in the DSC thermograms (Figure 4.23(a)), in addition to the beta phase, and it is known that the gamma phase interferes with the beta phase in FTIR. The beta phase was also increased in M2 (0.4% Ag-NPs and 1% cellulose).

4.2. 3. Investigation of β-phase content in the samples (by XRD)

The peaks that characterize each phase of PVDF in the XRD spectrum are listed in Table 4.8. Most of these peaks are around 20^o, so it is difficult to use the XRD technique alone to investigate the

PVDF phases; it is usually used in combination with FTIR. The values of 2θ are used interchangeably between the gamma and alpha phases in the region 19.9 to 20.5^{o}, which can lead to some confusion. The preparation technique has direct effect, not only on the phase content, but also on the compactness (Figure 4.28). Two samples were prepared from pure PVDF, one with a drum and the other with a rotating disk as a collector, and both of them contained β-phase crystals. The value of 2θ in the sample prepared by using the drum is lower than the value of 2θ for the sample prepared by using the rotating disk. According to equation (8), decreases in 2θ show increases in the internal distance (d), so it becomes less compact. The morphology difference between the two samples prepared by electrospinning with the drum and the rotating disk is shown in Figure 4.29.

Table 4.8. the 2θ for α-, β-, and γ-phases of PVDF
The values were obtained from ref [2, 89]

	α-phase	β-phase	γ-phase
2θ (degree)	17.66^{o}	20.26^{o}	18.5^{o}
	18.3^{o}		19.2^{o}
	19.9		20.04^{o}
	26.56^{o}		26.8^{o}
	39.5^{o}		

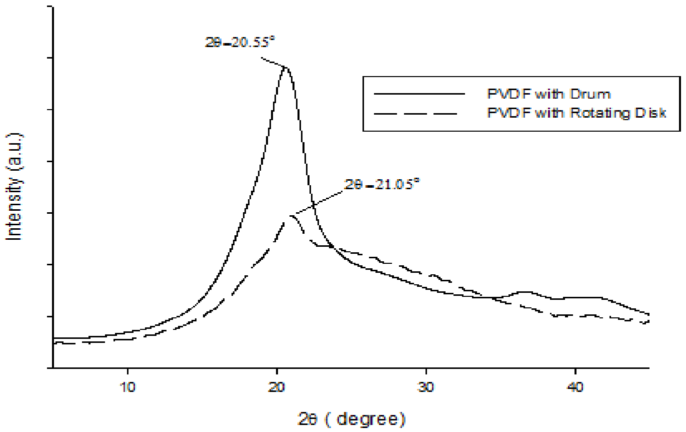

Figure 4.28. XRD spectra of electrospun PVDF films by drum and rotating disk

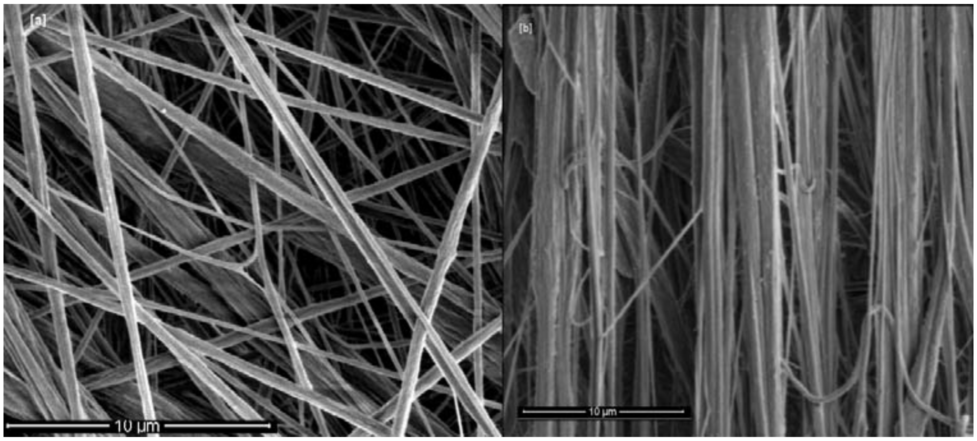

Figure 4.29. SEM micrographs of PVDF nanofibers fabricated by [a] drum, [b] rotating disk

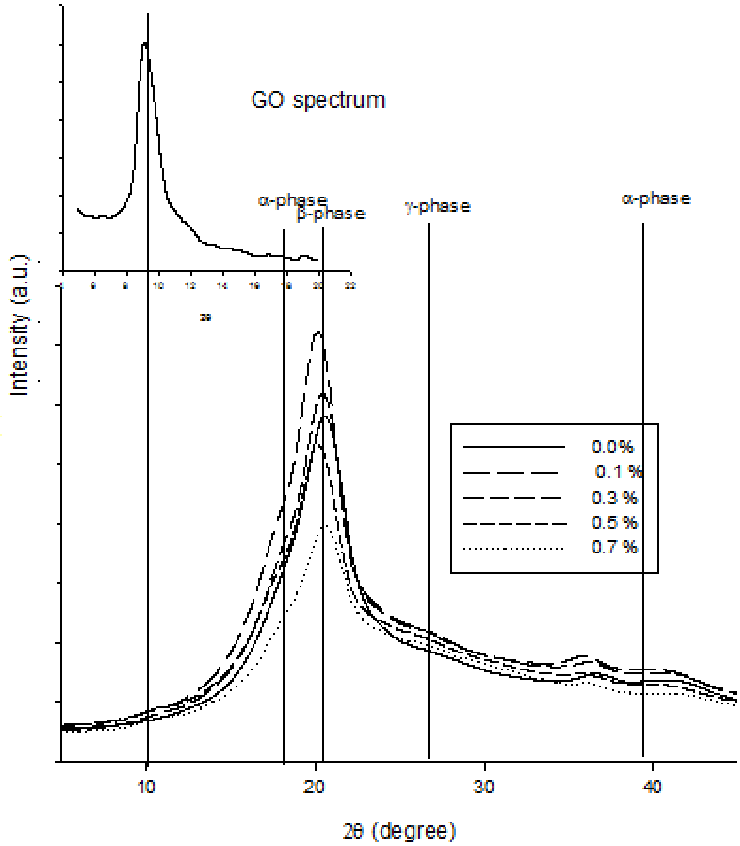

Figure 4.30. XRD spectra of electrospun PVDF/GO films by drum

Figure 4.30 shows that the main phase in the PVDF/GO films is the β-phase, but the α-phase and limited γ-phase are also presented. The highest peak for the β-phase is noticed at 0.1% of GO concentration. The result confirms the previous FTIR results. The GO peak observed at 9.1^{o} completely disappeared due to interaction with PVDF (Figure 4.30).

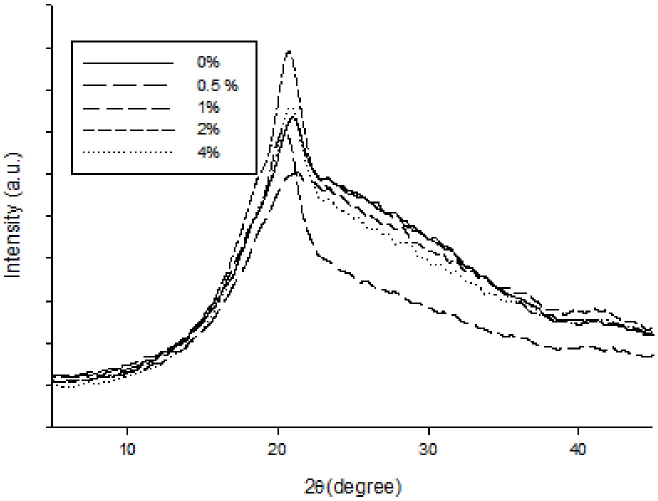

Figure 4.31. XRD spectra of electrospun PVDF/cellulose films by rotating disk

Figure 4.31 shows the XRD spectra of the PVDF/cellulose. It indicates that the intensity of the beta phase decreased at 0.5% cellulose, reached a maximum at 1 and 2%, and decreased again at 4%. To some extent this confirmed the FTIR results. It also shows that the gamma phase at 22.8^{o} and the alpha phase at 26.7^{o} were diminished at a concentration of 1% (Figure 4.31). These results are in line with the DSC and FTIR results.

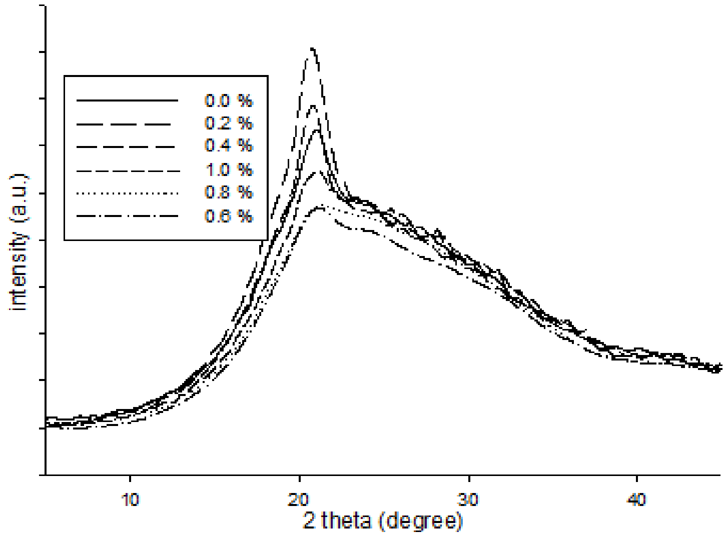

Figure 4.32. XRD spectra of electrospun PVDF/Ag-NPs films by rotating disk

Figure 4.32 shows the XRD spectra of PVDF/Ag-NPs, with 2θ having a maximum value of 20.66^{o} at a concentration of 0.2 % of Ag-NPs, which represents the maximum beta phase. This is different from the 0.5% obtained by FTIR. It is also noticed that, as the beta concentration increased, the position of the 2θ shifted to lower values, or the composites became less compact, and this was observed for all the composites. This makes sense because of the repulsion force between the fluorine atoms.

The maximum beta phase was observed in mixture 2, which was composed from 0.4% Ag-NPs, and 1% cellulose in PVDF (Figure 4.33). The beta phase content in the mixtures is close to that of pure PVDF, but they are less compact than the pure PVDF. There are also differences in the area of the gamma phase (at 22.8^{o}).

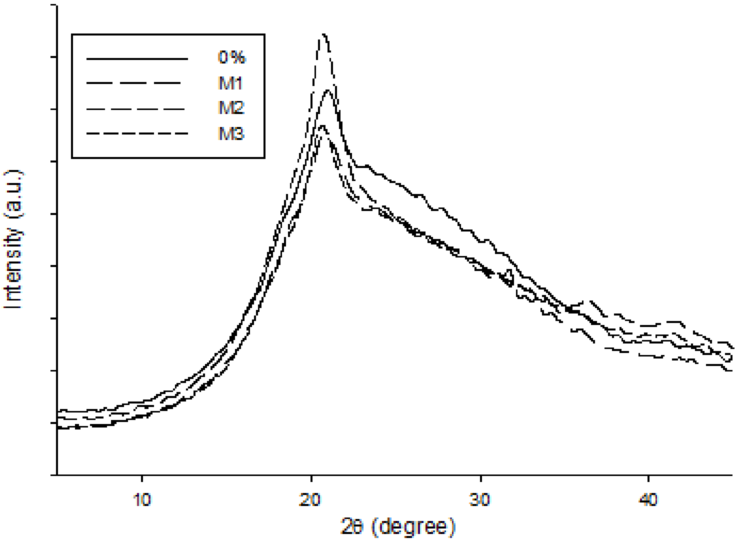

Figure 4.33. XRD spectra of the mixtures

4. 3. Thermal stability

The thermal stability was studied for all the composites individually and is shown in figure 4.34. For The GO started to lose its weight at room temperature before starting the program due to the presence of water in its crystals, and then it decomposed in two steps, first at 170 ℃ due to the removal of the –OH groups and second at 235 °C, due to the removal of C=O. Other references reported that the GO decomposed in one step above 200 ℃ [86], which could be due to the oxygen content in GO as a result of the preparation process. They used heating at 60 °C for 48 hours in a vacuum oven to dry the GO, but in our work we only dried it at ambient conditions. Using of heat probably led to the removal of the crystalline water and some hydroxyl groups, which is also clear from the differences in the weight lost percentages.

The decomposition of PVDF shows a weight lost percentage around 59 %, and this corresponds to the loss of two molecules of HF, where the percentage of HF was calculated theoretically by equation (10).

$$w_{HF}\ \% = \frac{W_{HF}}{W_{VDF}}\ x\ 100 - - - - - - - - - - - - - - - - - - (10)$$

where w_{HF} *%* is the weight percentage of HF in the vinylidene fluoride molecule, w_{HF} is the molecular weight of the HF equal to 20 amu, and W_{VDF} is the molecular weight of the vinylidene fluoride molecule equal to 64 amu. So $2(w_{HF\ \%})$= $\frac{2\ x\ 20}{64}$ x 100= 62.5 % . Botelho et al. [90], who studied the mechanism of thermal degradation of PVDF by using UV spectrometry linked to TGA and they, obtained similar results.

The PVDF/GO composite stabilities -shown in figure 3.34(a)- are generally improved with increasing the amount of GO, where the temperature at 30% mass loss of PVDF/GO is 10 °C higher than that of pure PVDF. This is due to the formation of char inside the sample which acted as a thermal barrier [91]. In addition, there is a small decomposition step starting at 100 °C due to the evaporation of absorbed water or some hydroxyl groups in GO.

Figure 4.34(b) shows the TGA thermograms of PVDF/cellulose. The samples decomposed in two steps, corresponding to the decomposition of cellulose at 350 °C, and the decomposition of PVDF at 464 °C. The samples with cellulose concentrations of 0, 0.5, 2 and 4% respectively show weight losses of 3, 3.5, 5, and 7%, which correlates well with the real concentrations of cellulose in the samples, except for 3% due to presence of moisture. Table 4.9 shows the temperatures at 30% weight loss, and the sample with 1% cellulose shows the highest thermal stability. The increase in thermal stabilities is probably due to the formation of char which resulted from the decomposition of the cellulose particles [91].

Figure 4.34(c) shows the TGA thermograms of PVDF/Ag-NPs composites, and the thermal stability was generally enhanced by adding Ag-NPs. The thermal stability of silver nanoparticles containing composites can be the result of (i) immobilization of the polymer and free radical chains through interaction with the Ag-NPs, or (ii) interaction between the degradation volatiles and the Ag-NPs which retarded the diffusion of these volatiles out of the polymer. It was, however, found that at high silver nanoparticle concentrations, the silver nanoparticles facilitated the thermal decomposition of PVDF due to their high thermal conductivity [42].

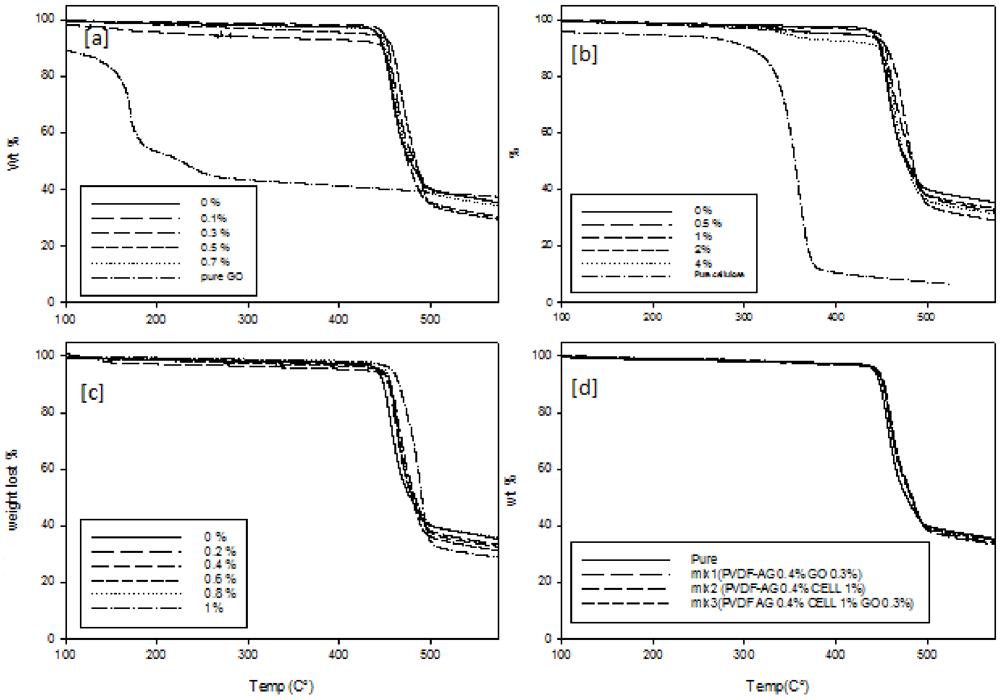

Figure 4.34. TGA thermograms of [a] GO/PVDF, [b] cellulose/PVDF, [c] Ag-NPs/PVDF composites, [d] mixtures

In the mixtures, the thermal stability increased with adding of the fillers as expected, where all fillers increase the thermal stability. The maximum shift is 4.7 °C from pure PVDF for mixture 1 (0.4% Ag-NPs and 0.3% GO) table 4.9.

Table 4.9. Temperatures at 30% mass loss for the different samples

GO/PVDF		Cellulose/PVDF		Ag-NPs/PVDF		Mixtures	
C %	T °C	C %	T °C	C %	T °C	C %	T °C
0.0	459.73	0.0	459.73	0.0	459.73	0	459.73
0.1	467.70	0.5	466.26	0.2	464.78	Mix 1	464.44
0.3	471.25	1.0	472.95	0.4	468.01	Mix 2	463.75
0.5	469.10	2.0	460.78	0.6	465.73	Mix 3	462.86
0.7	469.90	4.0	463.46	0.8	466.17		
GO	169.23			1.0	481.09		

C refers to concentration of filler in PVDF, and T refers to the temperature

4. 4. Mechanical properties

Most of the previous work showed that the tensile strength of PVDF increased with the addition of GO, and that there was a jump in tensile strength at 0.1% [36]. Some researchers, however, found that the tensile strength have a maximum at 0.15 % GO [28]. The reason for this difference is probably because they used different increments (0.05 %) and additives range (0 to 0.3%) for GO as well as different preparation technique. Our results showed that the tensile strength initially increased to a around 7 MPa at 0.1% GO, then decreased to less than 5 MPa at 0.5% GO, and then increased again (Figure 4.35). < note :- in general, the tensile strength was increased with increasing the concentration of GO, but there are a (Jump)at 0.5 % of GO due to improvement in crystallinity at this concentration.>

<note ;- error bar depends on the mean value and standard deviation>

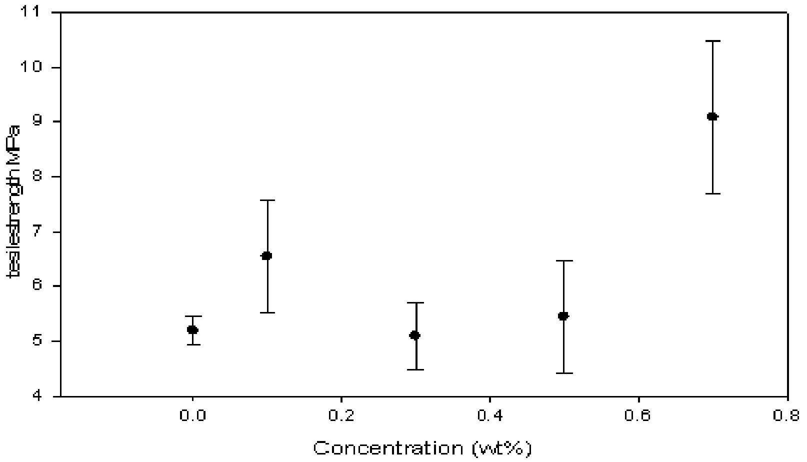

Figure 4.35. tensile test of GO/PVDF composites with different concentration

Figure 4.36 shows that the tensile strength increased with increasing cellulose content until a certain limit, which was 1% cellulose. Researchers who used PVDF to improve the mechanical properties of cellulose film, found that (i) the PVDF content should be less than 20% to give better improvement, (ii) as the amount of the PVDF increased, the tensile strength decreased, and (iii) pure PVDF had a very low tensile strength of about 2 MPa, and for 20% cellulose/PVDF it was 3 MPa [92].

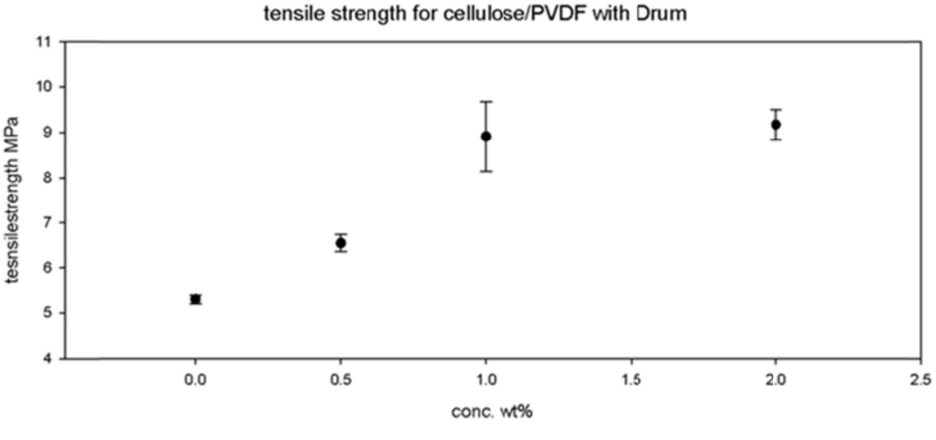

Figure 4.36. Tensile strengths of PVDF/cellulose composites with different concentration cellulose concentrations

Figure 4.37 shows that the addition of silver nanoparticles gradually increased the tensile strength with increasing Ag-NPs concentration. The tensile strength at 0.4% seems to be higher than expected, probably because the crystallinity of PVDF/Ag-NPs shows a maximum value at 0.4% Ag-NPs. These results show fairly large standard deviations because the tested samples were fibre mats with a non-uniform distribution of fiber thicknesses and defects. The Chae group reported that the mechanical properties of PVDF/Ag-NPs increased with the addition of silver until an Ag-NP concentration of 1%, then decreased at higher nanoparticle contents due to agglomeration of the Ag-NPs, and did not adhere well with the polymer [42].

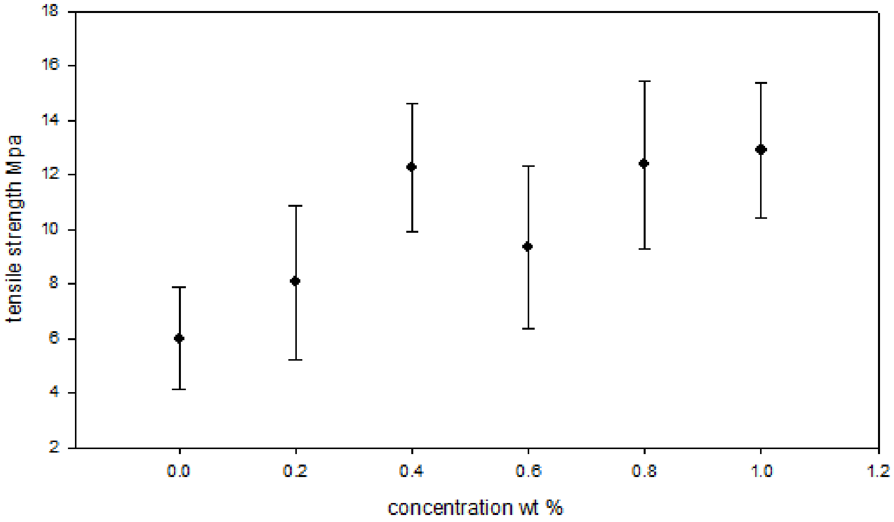

Figure 4.37. Tensile strengths of PVDF/cellulose composites with different concentration AgNPs concentrations

Table 4.10. Tensile strength values of Mixtures and PVDF with salts

Code	T1 MPa	T2 MPa	T3 MPa	T4 MPa	T Mean MPa
PVDF	7.17	6.95	3.85	-	6.0
PVDF-AG 0.4% GO 0.3%	6.5	6.2	7.4	8.1	7.1
PVDF-AG 0.4% CELL 1%	9.3	4.2	4.9	7.3	6.5
Ag 0.4% Cell 1% GO	9.3	11.7	9.2	9.7	10.0
0.5 NaCl	10.1	9.9	9.3	9.3	9.6
0.5 TEAC	8.6	4.2	5.9	4.5	5.8
T1, T2, T3, and T4 are trial 1,2,3 and4 respectively, T Mean is mean value of tensile strength					

Table 4.10 shows that the tensile strengths of the mixtures and the PVDF with salts were mostly higher than those of the neat PVDF, except for PVDF/TEAC.

4. 5. Dynamic mechanical analysis (DMA)

Figure 4.38(a) shows the storage modulus (G’) of the PVDF/GO composites. It shows that the mechanical properties of these composites were only slightly influenced with the addition of 0.1% GO particles. However, the addition of 0.3% of GO particles caused the significant improvement in the mechanical properties (from 2.37 x 10^7 to 4.08 x 10^7 Pa at frequency 0.1 Hz) and the improvement increased with further addition of GO. This was firstly due to the considerable stiffness of the GO sheets, and secondly due to the good interaction between the GO and PVDF which immobilized the polymer chains. The loss modulus (G”) did not show a glass transition as can be seen in figure 4.38 (b), and it followed the usual trend with increasing content of GO. PVDF with 0.7% of GO shows a considerably reduced loss modulus, which is most probably connected to the improved mechanical energy distribution within the material.

Figure 4.39 (a) for PVDF/cellulose nanofibres shows similar behavior as was observed in the case of GO. The storage modulus increased with increasing filler content. In this case, there was no optimum loading and the G” also increased with increasing additive content and does not exhibit the significant decrease as observed in the case of GO.

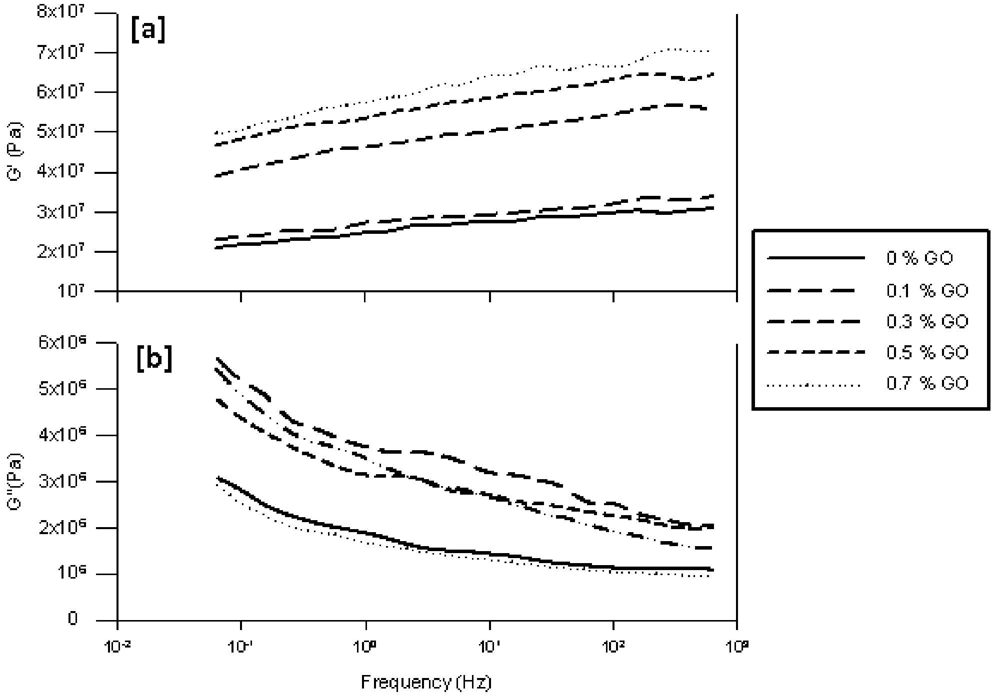

Figure 42.38 DMA results for PVDF/GO where [a] storage modulus and [b] loss modulus

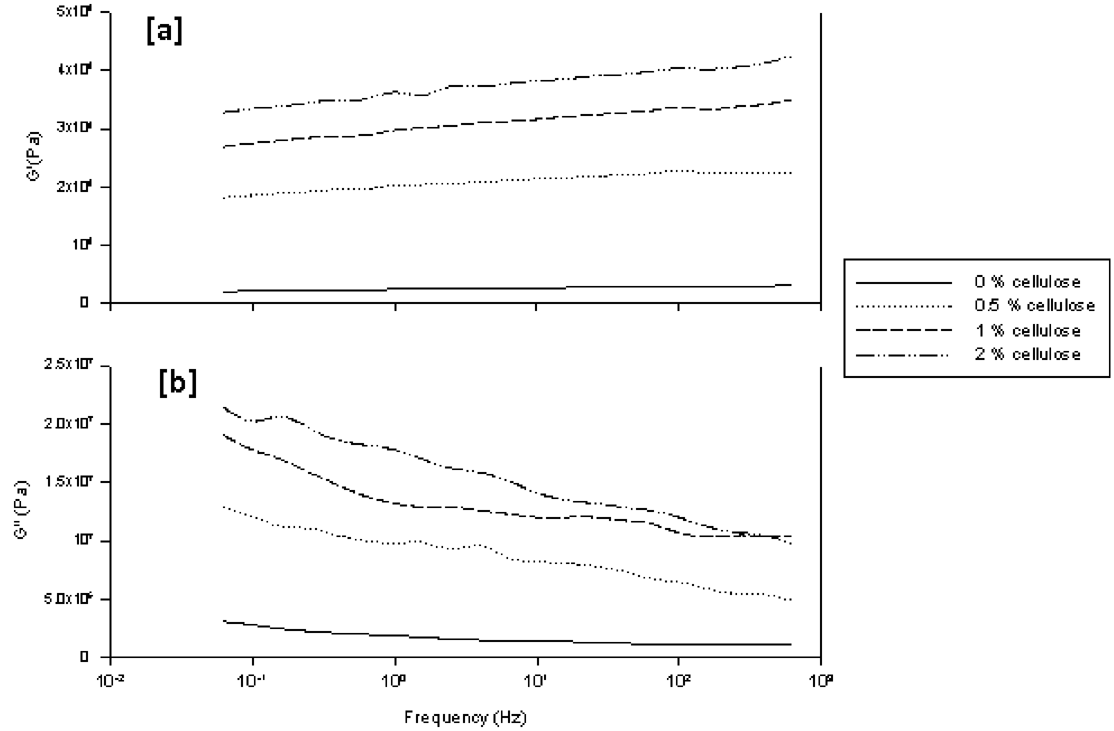

Figure 4.39 DMA results for PVDF/cellulose where [a] storage modulus and [b] loss modulus

Figure 4.40 shows the DMA results of PVDF/Ag-NPs composites. The storage modulus improved with the addition of a concentration of 0.2%. and the G’ for the concentrations of 0.2, 0.4 and 0.6% are very close to each other, and increased with further addition of Ag-NPs. In this case the also the G” curve also shows no glass transition. It is noticed that the storage modulus shows the largest difference at the concentration which give the maximum crystallinity by DSC. This expected due to influence of the crystallinity on the mechanical properties of the material.

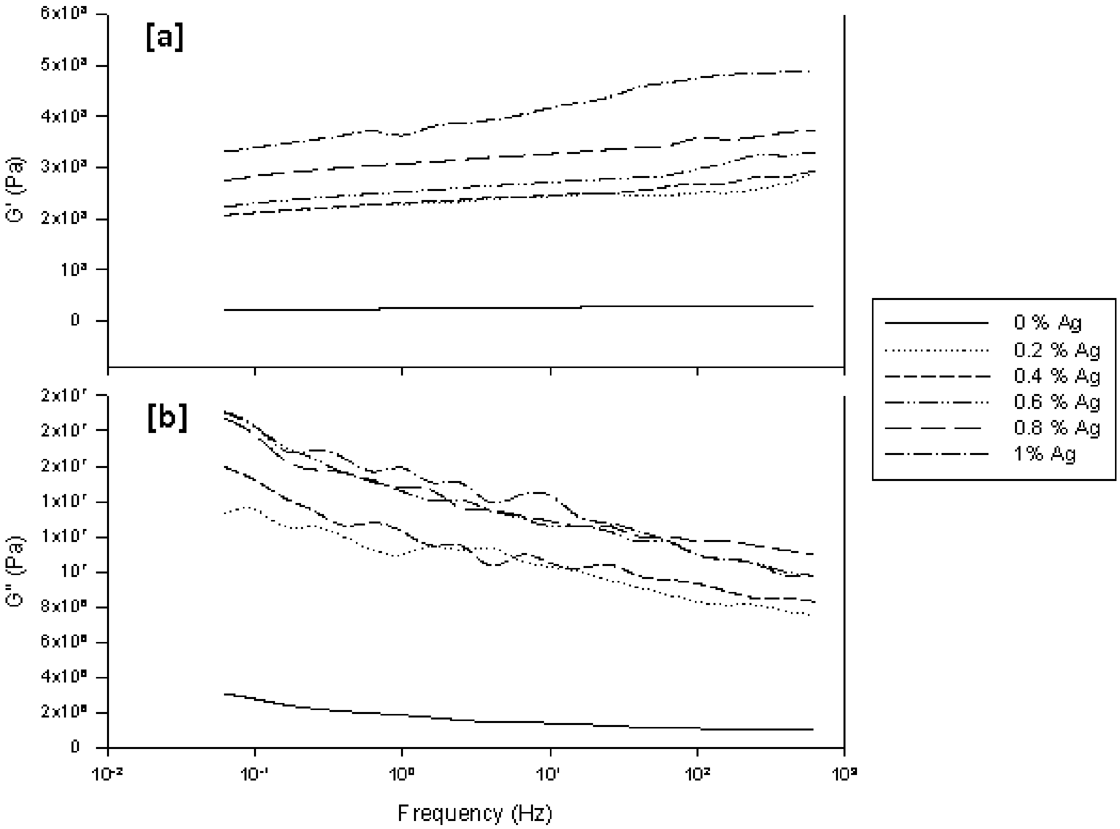

Figure 4.40 The DMA results for PVDF/AG-NPS composites where [a] storage modulus and [b] loss modulus

4. 6. Dielectric analysis

Figure 4.41 shows the alternative current (AC) conductivity of PVDF and its composites, the conductivity of PVDF/GO (Figure 4.41-a) increased with the addition of GO, because

GO has a slightly higher conductivity (6 x10^{-6} S/cm) than PVDF [93]. The conductivity of PVDF/cellulose did not show noticeable changes as seen in Figure 4.41(b), due to the comparable conductivity of cellulose and PVDF. However, in the case of Ag-NPs the conductivity of the composite films increased, due to the high conductivity of the Ag-NPs, as shown in Figure 4.41(c).

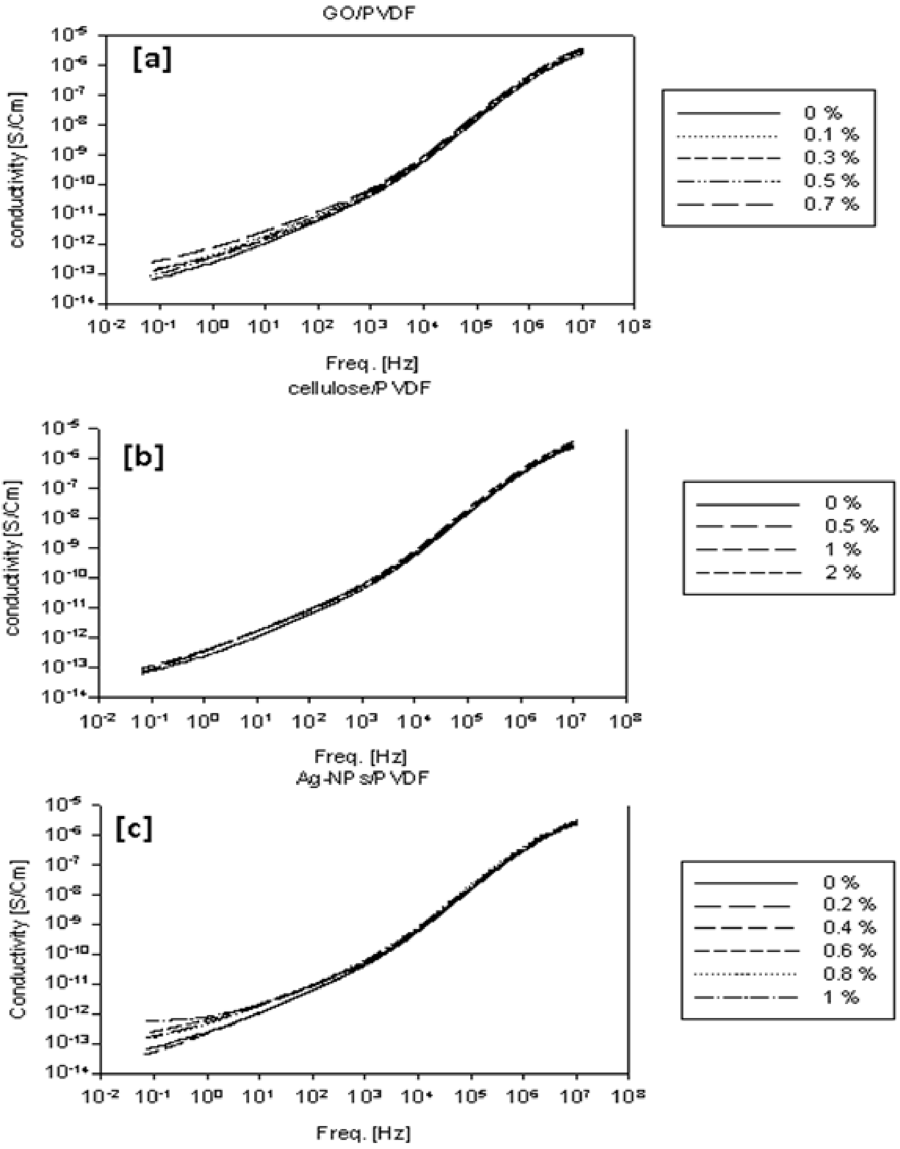

Figure 4.41 Conductivities of [a] PVDF/GO, [b] PVDF/cellulose, and [c] PVDF/Ag-NPs

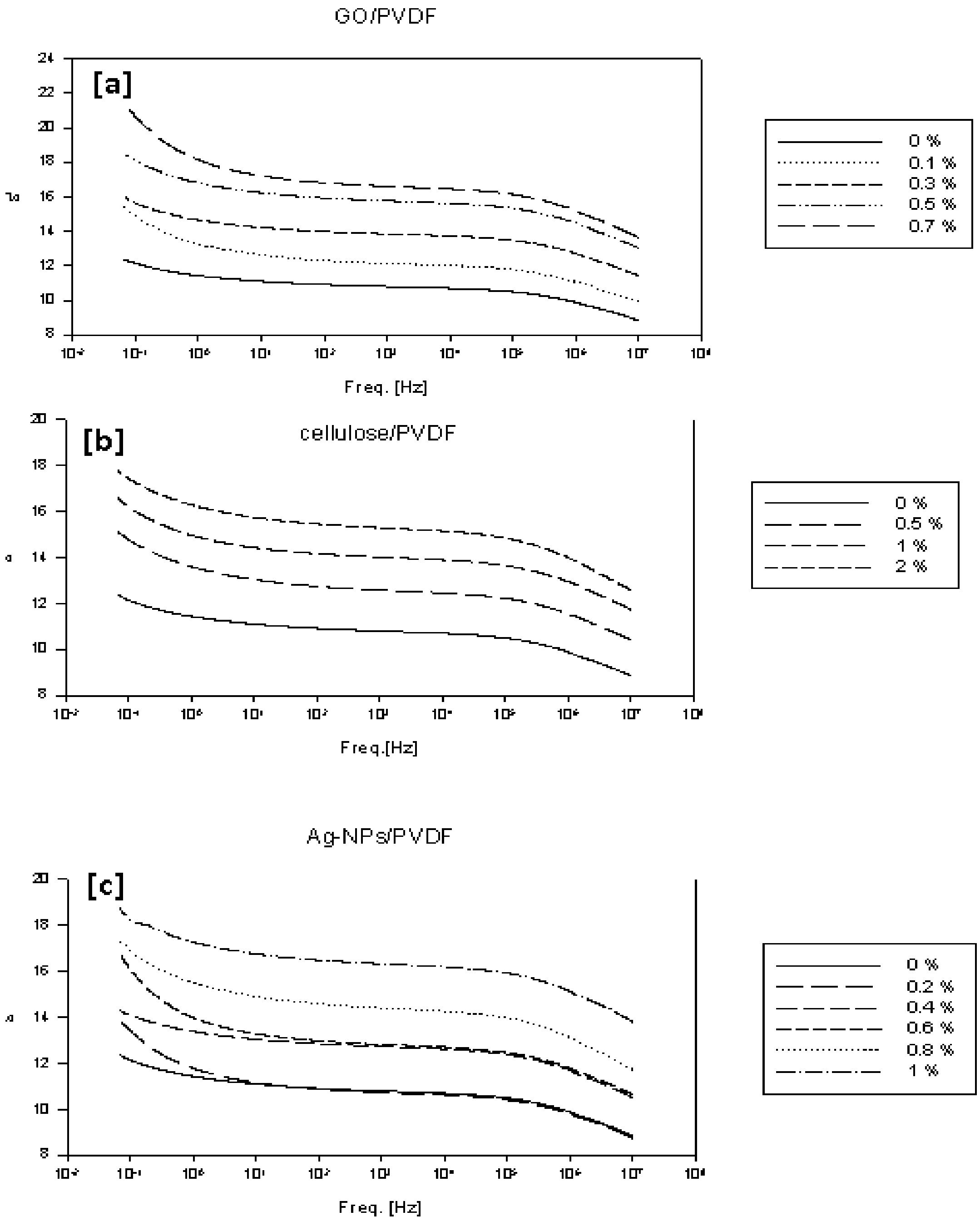

Figure 4.42 Storage moduli of [a] PVDF/GO, [b] PVDF/cellulose, and [c] PVDF/Ag-NPs

Figure 4.42 shows the relative permittivity of the PVDF composites. It is evident that it increased with the addition of fillers due to the accumulation of charges on the interface between the GO particles and the polymer during the current pass, most probably due to the Maxwell-Wagner-Sillar (MWS) interfacial polarization [94]. The relative permittivity shows higher values at low frequencies due to the mentioned MWS polarization, and with increasing amount of the additives (GO, Cellulose, AG-NPs) it further increases. It further exhibits a plateau from 10 to 10000 Hz, which is usual behavior for polymer and polymer composite materials [94].

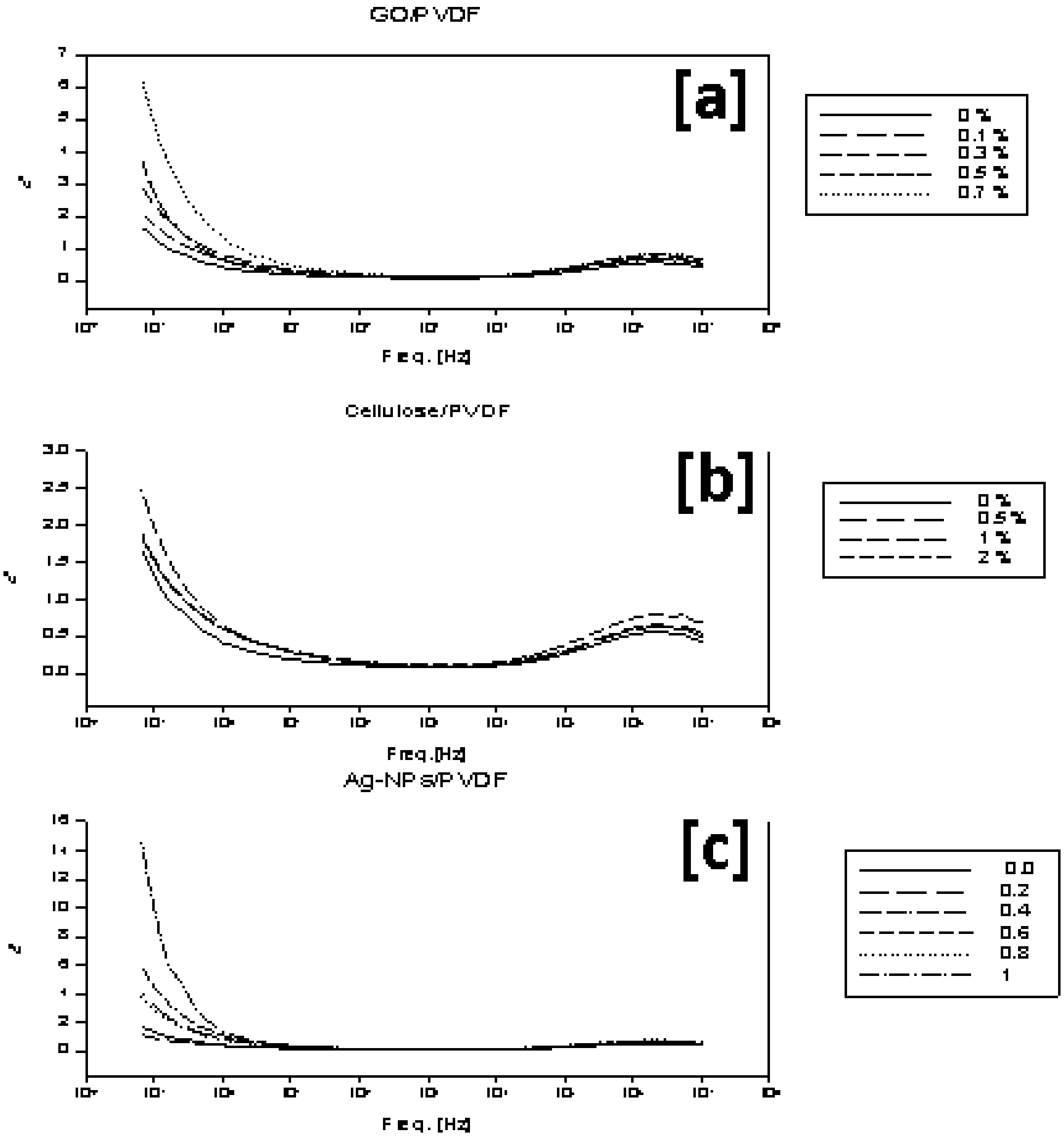

Figure 4.43 Dissipation factors of [a] PVDF/GO, [b] PVDF/cellulose, and [c] PVDF/Ag-NPs

For the dielectric losses (Figure 4.43), the dielectric loss factor follows the trend of the other dielectric investigations, which is expected for these materials. The only special case can be seen in Figure 4.43c, where the loss significantly increased with at amount of the AgNPs. This rapid increase from 1 to 14 at 0.1 Hz is again connected to the conductivity since the dielectric loss factor mostly represents the conductivity component of the sample.

Chapter 5. Conclusions

The current work produced PVDF nanofiber by electrospinning and showed that the addition of the fillers (GO, cellulose, and Ag-NPs) as well as the salts (NaCl and TEAC) changed the morphology, crystallinity, and the beta phase content of PVDF, and hence the physical and the mechanical properties. The enhancement is important for different applications such as Energy harvesting, energy storage, sensors, actuators, and the artificial muscles.

The morphology investigation of the samples revealed the following observations (i) the diameters of the produced fibers is dependent on the filler type and on the conductivity of the electrospinning solution. and the results showed that the fiber diameters decreased with the addition of Ag-NPs from 600 nm in pure PVDF to less than 200 nm at a concentration of 1.4 % of Ag-NPs, (ii) the importance of the solvent selection, where the solvent controlled the solution viscosity and the drying time of the nanofiber, choosing the DMF/acetone is right selection due to production of nanofibers at room temperature with high output quantity, (iii) the adjustment of the concentration of the PVDF solution can lead to electrospray or electrospinning, (iv) using the salts led to a decrease in the fibers diameters, independent of whether it is organic or inorganic, Where using 0.5 % of TEAC leads to decrease the fibers diameters from 600 nm to 230 nm, but in the case of inorganic salts, the mean value of fibers diameters is 250 nm at 0.5 % of NaCl, due to their solubility, and (v) aligned fibers can be obtained by using a rotating disk.

The study of the crystallinity showed an improvement in the degree of the crystallinity due to the presence of the fillers or the salts, as they can act as nucleating agents, and each filler had a specific concentration that gave a maximum crystallinity, which was 0.3, 0.5 and 0.4% for GO, cellulose, and Ag-NPs respectively, and this concentration led to crystallinity improvements of respectively 20, 3.5, and 8.7 %. Increasing the concentrations more than these values decrease the crystallinity due to aggregation or agglomeration of the fillers. The study of the crystallinity of the PVDF/salts showed the existence of a gamma phase which increased after thermal treatment.

The study of the β-phase content of the samples showed that there are two reasons for the enhancement of the beta content: i) the electrospinning process due to (a) shear force when the solution is forced through the needle, (b) the effect of electrostatic force, and (c) the mechanical force due to the high speed of the rotating disk or drum; (ii) the nature of the filler, where each filler has its own mechanism to attract the fluorine atoms; for the GO it depends on the functional groups that are rich with oxygen, for the cellulose it depends on the (-OH) group, and for Ag-NPs it depends on the electrons on the surface of the nanoparticles. FTIR and XRD were used to determine the β-phase content, and the results of these two techniques were in good agreement. Each filler had its own concentration that gave the maximum value of the β-phase, which was 0.1, 1 and 0.5% for GO, cellulose, and Ag-NPs respectively.

The thermal studies showed that the melting points depend on the crystal size in the matrix not on the filler type, where all the samples had similar melting points with changing the filler or the concentration, except in the case of the salts. The recrystallization temperatures showed an increase in the crystallization temperatures with increasing the concentration, regardless of the nature of the filler. The thermal decomposition behavior of the samples show that (i) all the samples had a decomposition temperature above that of pure PVDF at 30% mass loss, (ii) the cellulose additive start to decompose before the PVDF, and (iii) silver nanoparticles enhanced the thermal stability up to a concentration of 5%.

The tensile tests showed an improvement in the tensile strengths of the PVDF composites with addition of the fillers, and the maximum values were 75.5, 69.8, and 100 % at concentrations 0.7, 1.0, and 1 % of GO, cellulose , and Ag-NPs respectively.

DMA analysis of the PVDF composites with the fillers (GO, cellulose, and Ag-NPs) show the improvement in storage modulus (G') with adding the filler. And there is a significant increase in G' at a specific concentration of each filler, at 0.3, 0.5, and 0.2 % of GO, cellulose, and Ag-NPs respectively. The loss modulus (G") for all the samples does not show the glass transition temperature (Tg).

The dielectric analysis study of the prepared samples shows that (i) the alternating current (AC) conductivities of the GO and Ag-NPS nanocomposites increased with increasing the concentration of the fillers at low frequency (0.1 Hz), especially in the case of AG-NPS due to it is conductive behavior. Cellulose didn't affect the conductivity as it is not a conductive material. The relative permittivity (ε') study shows the improvement in the (ε') of the PVDF as general with adding the filers from 12 to around 18 at frequency of 1Hz, and this improvement will increase the capacitance of the capacitor if this material is used in energy storage. Also the loss moduli (ε")show that , the loss modulus of GO and cellulose increased very slowly with addition of the fillers, but in the case of Ag-NPs, the (ε") increased rapidly with addition of silver, and thus due to conductivity effect.

Limitations

- ✓ Going wide, studying many variables in the same time, instead of focusing on specific variables.

- ✓ Electrospinning, which has many parameters to control, and some of them such as the humidity and surrounding temperature are out of control and it is a time consuming technique.

Suggestions for future work

1- GO is a promising material – study of the effect of the processing technique on the beta phase of PVDF/GO.

2- Identify different types of GO (with different content of Oxygen) on the physical and mechanical properties of the nanofibres.

3- Study the effect of the processing parameters with time, on the crystallinity and beta-phase of the PVDF nanofibres.

Study the effect of the particle size of Ag-NPs on the physical-mechanical parameters of PVDF composites.

References

1. Liu, F., et al., *Progress in the production and modification of PVDF membranes.* Journal of Membrane Science, 2011. **375**: p. 1-27.
2. P. Martinsa, A.C. Lopesa, and S. Lanceros-Mendez, *Electroactive phases of poly(vinylidene fluoride): Determination, processing and applications.* Progress in Polymer Science, 2014. **39**: p. 683-706.
3. Guo-dong Kangn and Y.-m. Cao, *Application and modification of poly(vinylidene fluoride) (PVDF) membranes – A review.* Journal of Membrane Science, 2014. **463**: p. 145-165.
4. Giannett, E., *Semi-crystalline fluorinated polymers.* polymer international, 2001. **50**: p. 10-26.
5. Rajesh, P.S.M., et al., *Enhancing Beta-Phase in PVDF through Physicochemical Modification of Cellulose.* Electron. Mater. Lett.,, 2014. **10**(1): p. 315-319.
6. Xia, S. and M. Ni, *Preparation of poly(vinylidene fluoride) membranes with graphene oxide addition for natural organic matter removal.* Journal of Membrane Science, 2015. **473**(0): p. 54-62.
7. Ting Maa, et al., *Preparation of PVDF based blend microporous membranes for lithium ion batteries by thermally induced phase separation: I. Effect of PMMA on the membrane formation process and the properties.* Journal of Membrane Science, 2013. **444**: p. 213-222.
8. Figoli, A., et al., *Hollow fibers for seawater desalination from blends of PVDF with different molecular weights: Morphology, properties and VMD performance.* Polymer, 2014. **55**: p. 1296-1306.
9. GaeDe´tan Laroche, et al., *Identification and quantification of the crystalline structures of poly(vinylidene fluoride) sutures by wide-angle X-ray scattering and differential scanning calorimetry.* 1997.
10. Kakimoto, K.-i., K. Fukata, and H. Ogawab, *Fabrication of fibrous BaTiO3-reinforced PVDF composite sheet for transducer application.* Sensors and Actuators A, 2013. **200**: p. 21- 25.
11. Chen, D., T. Sharma, and J.X.J. Zhang, *Mesoporous surface control of PVDF thin films for enhanced piezoelectric energy generation.* Sensors and Actuators A, 2014. **216**: p. 196-201.
12. Li, B., et al., *Sensitivity of Pressure Sensors Enhanced by Doping Silver Nanowires.* Sensors, 2014. **14**(9889-9899).
13. Pérez, R., M. Král, and H. Bleuler, *Study of polyvinylidene fluoride (PVDF) based bimorph actuators for laser scanning actuation at kHz frequency range.* Sensors and Actuators, 2012. **A 183**: p. 84- 94.
14. Phule, A.D., S. Ram, and A.K. Tyagi, *Tailoring absorption and emission of light in dielectric polymer nanofluids of reinforced poly(vinylidene fluoride) with silver nanoparticles.* Journal of Applied Physics, 2010. **107**(3).
15. Bodkhe, S., et al., *Beta-phase enhancement in polyvinylidene fluoride through filler addition: comparing cellulose with carbon nanotubes and clay.* J Polym Res, 2014. **21**.
16. A. Salimi and A.A. Yousefi, *Analysis Method FTIR studies of β-phase crystal formation in stretched PVDF films.* Polymer Testing, 2003. **22**: p. 699-704.
17. Miranda, D., et al., *Influence of silver nanoparticles concentration on the α-to β-phase transformation and the physical properties of silver nanoparticles doped poly(vinylidene fluoride) nanocomposites.* Journal of Nanoscience and Nanotechnology, 2009. **9**(5): p. 2910-2916.
18. Yi-Yuan Chiua, et al., *Development of a piezoelectric polyvinylidene fluoride (PVDF) polymer-based sensor patch for simultaneous heartbeat and respiration monitoring.* Sensors and Actuators A, 2013. **189**: p. 328- 334.
19. Merlini, C., et al., *Development of a novel pressure sensing material based on polypyrrole-coated electrospun poly(vinylidene fluoride) fibers.* Materials Science and Engineering: B, 2014. **179**(0): p. 52-59.
20. Mandal, D., K. Henkel, and D. Schmeisser, *Comment on "preparation and characterization of silver-poly(vinylidene fluoride) nanocomposites: Formation of piezoelectric polymorph of poly(vinylidene fluoride)".* Journal of Physical Chemistry B, 2011. **115**(35): p. 10567-10569.
21. Li, B., J. Zheng, and C. Xu. *Silver nanowire dopant enhancing piezoelectricity of electrospun PVDF nanofiber web*. in *Proceedings of SPIE - The International Society for Optical Engineering*. 2013.

22. Shotton, K.C., D.R. Bacon, and R.M. Quilliam, *A pvdf membrane hydrophone for operation in the range 0.5 Mhz to 15 Mhz.* Ultrasonics, 1980. **18**(3): p. 123-6.
23. González-Morán, C.O., C.J. Rodríguez-Montoya, and E. Suaste-Gómez. *Preparation of membranes of poly(vynilidene fluoride) as temperature sensors via electrospinning for biomedical applications*. in *Program and Abstract Book - 2010 7th International Conference on Electrical Engineering, Computing Science and Automatic Control, CCE 2010*. 2010.
24. Edward Bormashenko , et al., *Polyvinylidene fluoride—piezoelectric polymer for integrated infrared optics applications.* Optical Materials, 2004. **27**: p. 429-434.
25. Xie, X.D., Q. Wangb, and N. Wub, *Energy harvesting from transverse ocean waves by a piezoelectric plate.* International Journal of Engineering Science, 2014. **81**: p. 41-48.
26. Chang, J., et al., *Piezoelectric nanofibers for energy scavenging applications.* Nano Energy, 2012: p. 356-371.
27. Nunes-Pereira, J., et al., *Energy harvesting performance of piezoelectric electrospun polymer fibers and polymer/ceramic composites.* Sensors and Actuators A: Physical, 2013. **196**(0): p. 55-62.
28. Wang, Z., et al., *Novel GO-blended PVDF ultrafiltration membranes.* Desalination, 2012. **299**: p. 50-54.
29. Klinge, U., et al., *PVDF as a new polymer for the construction of surgical meshes.* Biomaterials, 2002. **23**(16): p. 3487-93.
30. Damaraju, S.M., et al., *Structural changes in PVDF fibers due to electrospinning and its effect on biological function.* Biomed Mater, 2013. **8**(4): p. 045007.
31. Inc, A. " *polyvinylidene fluoride Wire & Cable Applications" and "Fire-Resistant Foams for Pharmaceutical and Semiconductor Cleanrooms"*. Kynar® and Kynar Flex® brochures 2005 2014 [cited 2015 jan 2015]; this is a web site of the company fabricate the PVDF items in many fields (automotaive, ...)]. Available from: http://americas.kynar.com/en/literature/articles-reprints/index.html.
32. R. Gonçalves , P.M.M., C. Caparrós , P. Martins , M. Benelmekki a, G. Botelho , S. Lanceros-Mendez , A. Lasheras d, J. Gutiérrez , J.M. Barandiarán *Nucleation of the electroactive β-phase, dielectric and magnetic response of poly(vinylidene fluoride) composites with Fe2O3 nanoparticles.* Journal of Non-Crystalline Solids, 2013. **361**: p. 93-99.
33. Thakur, P., et al., *Effect of in situ synthesized Fe2O3 and Co3O4 nanoparticles on electroactive beta phase crystallization and dielectric properties of poly(vinylidene fluoride) thin films.* Phys Chem Chem Phys, 2015. **17**(2): p. 1368-78.
34. Li, Y., Y. Iwakura, and H. Shimizu, *Crystal form and phase structure of poly(vinylidene fluoride)/polyamide 11/clay nanocomposites by high-shear processing.* J Nanosci Nanotechnol, 2008. **8**(4): p. 1714-20.
35. Liu, Y.L., et al., *Cooperative effect of electrospinning and nanoclay on formation of polar crystalline phases in poly(vinylidene fluoride).* ACS Appl Mater Interfaces, 2010. **2**(6): p. 1759-68.
36. Achaby, M.E., et al., *Piezoelectric -polymorph formation and properties enhancement in graphene oxide – PVDF nanocomposite films.* Applied Surface Science, 2012. **258**: p. 7668- 7677.
37. Li, Y., et al., *Role of ion-dipole interactions in nucleation of gamma poly(vinylidene fluoride) in the presence of graphene oxide during melt crystallization.* J Phys Chem B, 2012. **116**(51): p. 14951-60.
38. Greco, T., F. Wang, and M. Wegener, *Multifunctional silver poly(vinylidene fluoride) nanocomposites: Nanoparticle synthesis, film processing, and structural characterization.* Ferroelectrics, 2010. **405**(1): p. 85-91.
39. Zhang, X., et al., *Dye-sensitized solar cell with energy storage function through PVDF/ZnO nanocomposite counter electrode.* Adv Mater, 2013. **25**(30): p. 4093-6.
40. Wang, G., *Enhanced dielectric properties of three-phase-percolative composites based on thermoplastic-ceramic matrix (BaTiO3 + PVDF) and ZnO radial nanostructures.* ACS Appl Mater Interfaces, 2010. **2**(5): p. 1290-3.
41. Vinogradov, A. and F. Holloway, *Electro-mechanical properties of the piezoelectric polymer PVDF.* Ferroelectrics, 1999. **226**(1): p. 169-181.

42. Chae, D.W., et al., *Influence of high contents of silver nanoparticles on the physical properties of poly(vinylidene fluoride).* Molecular Crystals and Liquid Crystals, 2007. **464**(1): p. 233-241.
43. Yang, J., et al., *Realizing the full nanofiller enhancement in melt-spun fibers of poly(vinylidene fluoride)/carbon nanotube composites.* Nanotechnology, 2011. **22**(35): p. 355707.
44. Shrivastava, S., et al., *Characterization of enhanced antibacterial effects of novel silver nanoparticles.* Nanotechnology, 2007. **18**.
45. Yuan, J., et al., *Electrospinning of antibacterial poly(vinylidene fluoride) nanofibers containing silver nanoparticles.* Journal of Applied Polymer Science, 2010. **116**(2): p. 668-672.
46. Liu, S., et al., *Antibacterial Activity of Graphite, Graphite Oxide, Graphene Oxide, and Reduced Graphene Oxide: Membrane and Oxidative Stress.* American Chemical Society, 2011. **VOL. 5**(NO. 9): p. 6971-6980.
47. Hossein Razzaghi, M., et al., *Morphological and separation performance study of PVDF/CA blend membranes.* Journal of Membrane Science, 2014. **470**(0): p. 547-557.
48. Li, J.H., et al., *The double effects of silver nanoparticles on the PVDF membrane: Surface hydrophilicity and antifouling performance.* Applied Surface Science, 2013. **265**: p. 663-670.
49. Rietveld, I.B., et al., *Morphology control of poly(vinylidene fluoride) thin film made with electrospray.* J Colloid Interface Sci, 2006. **298**(2): p. 639-51.
50. Okoshi, T., et al., *Microporous small diameter PVDF-TrFE vascular grafts fabricated by a spray phase inversion technique.* ASAIO J, 1992. **38**(3): p. M201-6.
51. Buonomenna, M.G., et al., *Combined emulsion and phase inversion techniques for the preparation of catalytic PVDF microcapsules.* J Phys Chem B, 2008. **112**(36): p. 11264-9.
52. Tao, M.M., F. Liu, and L.X. Xue, *Poly(vinylidene fluoride) membranes by an ultrasound assisted phase inversion method.* Ultrason Sonochem, 2013. **20**(1): p. 232-8.
53. Li, J.J., et al., *Formation of nanocrystalline copolymer thin film PVDF-TrFE and its ferroelectric electron emission property.* J Nanosci Nanotechnol, 2009. **9**(2): p. 832-5.
54. Smith, O.L., et al., *Enhanced permittivity and energy density in neat poly(vinylidene fluoride-trifluoroethylene-chlorotrifluoroethylene) terpolymer films through control of morphology.* ACS Appl Mater Interfaces, 2014. **6**(12): p. 9584-9.
55. Loordhuswamy, A.M., et al., *Fabrication of highly aligned fibrous scaffolds for tissue regeneration by centrifugal spinning technology.* Mater Sci Eng C Mater Biol Appl, 2014. **42**: p. 799-807.
56. Sun, B., et al., *Advances in three-dimensional nanofibrous macrostructures via electrospinning.* Progress in Polymer Science, 2014. **39**: p. 862-890.
57. Ding, B. and J. Yu, *Electrospun Nanofibers for Energy and Environmental Applications*. Nanostructure Science and Technology, ed. D.J. Lockwood. 2014: Springer.
58. Beachley, V. and X. Wen, *Polymer nanofibrous structures: Fabrication, biofunctionalization, and cell interactions.* Prog Polym Sci, 2010. **35**(7): p. 868-892.
59. Jayakumar, R. and S.V. Nair, *Biomedical Applications of Polymeric Nanofibers*, ed. M.V.B.V.G.W.U. Wiesner, et al. Vol. 246. 2012: Springer.
60. Taylor, T. and K. Schug. *Essential Guide to Electrospray Ionization (ESI) for LC-MS (Part 1)*. 2011; Available from: http://www.chromacademy.com/Electrospray-Ionization-ESI-for-LC-MS.html?tpm=1_1.
61. M. Zadeh, M. Keyanpour-Rad, and T. Ebadzadeh, *Effect of viscosity of polyvinyl alcohol solution on morphology of the electrospun mullite nanofibres.* Ceramics International, 2014. **40**(4): p. 5461-5466.
62. Li, Z. and C. Wang, *One-Dimensional nanostructures,Electrospinning Technique and Unique Nanofibers*. SPRINGER BRIEFS IN MATERIALS. 2013.
63. Matabola, K.P. and R.M. Moutloali, *The influence of electrospinning parameters on the morphology and diameter of poly(vinyledene fluoride) nanofibers- effect of sodium chloride.* 2013. **48**(16): p. 5475-5482.
64. Wang, J., et al., *Aligned assembly of nano and microscale polystyrene tubes with controlled morphology.* Polymer, 2014. **55**: p. 3008-3014.

65. Yee, W.A., et al., *Morphology, polymorphism behavior and molecular orientation of electrospun poly(vinylidene fluoride) fibers.* Polymer, 2007. **48**(2): p. 512-521.
66. Xiaomeng Sui, E.W., and H. Daniel Wagner∗, *Enhanced Mechanical Properties of Electrospun Nano-Fibers Through NaCl Mediation.* Journal of Nanoscience and Nanotechnology, 2011. **Vol. 11**: p. 7931-7936.
67. Liu, Z.H., et al., *Piezoelectric properties of PVDF/MWCNT nanofiber using near-field electrospinning.* Sensors and Actuators A, 2013. **193**: p. 13- 24.
68. Wang, S., et al., *Magnetic composite nanofibers fabricated by electrospinning of Fe3O4/gelatin aqueous solutions.* Materials Science and Engineering: B, 2014. **190**(0): p. 126-132.
69. Sung, Y.K., B.W. Ahn, and T.J. Kang, *Magnetic nanofibers with core (Fe3O4 nanoparticle suspension)/sheath (poly ethylene terephthalate) structure fabricated by coaxial electrospinning.* Journal of Magnetism and Magnetic Materials, 2012. **324**(6): p. 916-922.
70. Wang, H., et al., *Fabrication of aligned ferrite nanofibers by magnetic-field-assisted electrospinning coupled with oxygen plasma treatment.* Materials Research Bulletin, 2009. **44**(8): p. 1676-1680.
71. Iwaura, R., H. Minamikawa, and T. Shimizu, *Sodium chloride-induced self-assembly of microfibers from nanofiber components.* Journal of Colloid and Interface Science, 2004. **277**(2): p. 299-303.
72. Zhao, J., et al., *Preparation, structure and crystallinity of chitosan nano-fibers by a solid–liquid phase separation technique.* Carbohydrate Polymers, 2011. **83**(4): p. 1541-1546.
73. Layek, R.K., et al., *Enhancement of physical, mechanical, and gas barrier properties in noncovalently functionalized graphene oxide/poly(vinylidene fluoride) composites.* Carbon, 2015. **81**(0): p. 329-338.
74. Won-Chun Oh, et al., *The Effect of Thermal and Ultrasonic Treatment on the Formation of Graphene-oxide Nanosheets.* Journal of the Korean Physical Society, 2010. **56**(4): p. 1097∼1102.
75. Chen, Y., et al., *Functional poly(vinylidene fluoride) membrane anchored with silver nanoparticle with antibacterial activity.* Synthetic Metals, 2013. **174**(0): p. 1-5.
76. Silva, M.P., et al., *Extrusion of poly(vinylidene fluoride) recycled filaments: Effect of the processing cycles on the degree of crystallinity and electroactive phase content.* Polymer Testing, 2013. **32**: p. 1041-1044.
77. Ferreira, J.C.C., et al., *Variation of the physicochemical and morphological characteristics of solvent casted poly(vinylidene fluoride) along its binary phase diagram with dimethylformamide.* Journal of Non-Crystalline Solids, 2015. **412**(0): p. 16-23.
78. AlMaadeed, M.A., et al., *Date palm wood flour/glass fibre reinforced hybrid composites of recycled polypropylene: Mechanical and thermal properties.* Materials and Design, 2012. **42**: p. 289-294.
79. Wunderlich, B., *Thermal Analysis of Polymeric Materials*. 2005: Springer.
80. Park, Y.J., Y.S. Kang, and C. Park, *Micropatterning of semicrystalline poly(vinylidene fluoride) (PVDF) solutions.* European Polymer Journal, 2005. **41**: p. 1002-1012.
81. Sandler, S.R., et al., *Experiment 23 - Dynamic mechanical analysis*, in *Polymer Synthesis and Characterization*, S.R.S.K.-A.B.M. Pearce, Editor. 1998, Academic Press: San Diego. p. 198-206.
82. Zhang, F., et al., *Poly(vinylidene fluoride)/SiO2 composite membranes prepared by electrospinning and their excellent properties for nonwoven separators for lithium-ion batteries.* Journal of Power Sources, 2014. **251**(0): p. 423-431.
83. M. Essalhi and M. Khayet, *Self-sustained webs of polyvinylidene fluoride electrospun nanofibers at different electrospinning times Theoretical analysis, polarization effects and thermal efficiency.* Journal of Membrane Science, 2013. **433**: p. 180-191.
84. Truong, Y.B., et al., *Application of electrospun gas diffusion nanofibre-membranes in the determination of dissolved carbon dioxide.* Macromolecular Materials and Engineering, 2013. **298**(5): p. 590-596.
85. Shi, N., et al., *Crystal polymorphism and enhanced dielectric performance of composite nanofibers of poly(vinylidene fluoride) with silver nanoparticles.* Journal of Applied Polymer Science, 2013. **128**(2): p. 1004-1010.

86. Konios, D., et al., *Dispersion behaviour of graphene oxide and reduced graphene oxide.* Journal of Colloid and Interface Science, 2014. **430**(0): p. 108-112.
87. Kamide, K., et al., *Dissolution Process and Dissolved State of Cellulose in Dimethylformamide-Chloral-Pyridine System.* Polym J, 1980. **12**(8): p. 521-534.
88. An, N., et al., *Preparation and properties of β-phase graphene oxide/PVDF composite films.* Journal of Applied Polymer Science, 2015. **132**(10).
89. Tawansi, A., et al., *Physical properties and β-phase increment of AgNO3-filled poly(vinylidene fluoride) films.* Polymer International, 2004. **53**(4): p. 370-377.
90. Botelho, G., et al., *Relationship between processing conditions, defects and thermal degradation of poly(vinylidene fluoride) in the β-phase.* Journal of Non-Crystalline Solids, 2008. **354**(1): p. 72-78.
91. Feng, Y., et al., *Thermal degradation mechanism and kinetics of polycarbonate/silica nanocomposites.* Polymer Degradation and Stability, 2014. **107**(0): p. 129-138.
92. Zhang, X., et al., *Preparation and characterization of regenerated cellulose/poly (vinylidene fluoride) (PVDF) blend films.* Carbohydr Polym, 2012. **89**(1): p. 67-71.
93. Zhang, W.L., et al., *Electrorheology of Graphene Oxide.* ACS Appl. Mater. Interfaces, 2012. **4** (4): p. 2267-2272.
94. Vasundhara, K., B.P. Mandal, and A.K. Tyagi, *Enhancement of dielectric permittivity and ferroelectricity of a modified cobalt nanoparticle and polyvinylidene fluoride based composite.* RSC Advances, 2015. **5**(12): p. 8591-8597.

APPENDIX

APPENDIX A. THE ACCEPTED ABSTRACT IN ICMAC 2015 CONFERENCE, BRISTOL, UK.

Effect of preparation techniques on

PVDF nanofibers and nano-composites

A. Issa[1*], M.A. AlMaadeed[1,2], M. Mrlík[2], E. J. Thekkethottiyil[2]
[1]Materials Science and Technology Program,
[2]Centre for Advanced Materials,
Qatar University, P. O. BOX 2713, Doha, Qatar.
ahmedissa@qu.edu.qa

SUMMARY

This work aims to prepare PVDF composite nanofibers with uniaxial alignment using electrospinning. Different variables such as concentration of the filler and collector shape are considered. The morphology is investigated and effect of polymer composition and the degree of nanofiber alignment on physical and mechanical properties are observed.

Keywords: electrospinning, conditions, nanofibers, PVDF, cellulose, Silver, graphene oxide, aligned nanofibers.

ABSTRACT

PolyVinylidene Fluoride (PVDF) is a low cost material with outstanding properties such as thermal stability, high flexibility, chemical resistance, good mechanical properties and biocompatibility. Many researchers have reported that the nanofibers with controlled shape and morphology have exceptional potential in energy harvesting, drug delivery systems and tissue engineering.

This work will explain how PVDF composite nanofibers were prepared by electrospinning with different additives viz. graphene oxide, cellulose and silver nanoparticles in different concentrations. Drum speed, voltage changes and effect of different additives changed the thickness and alignment of the resulting nanofibers. The following techniques were used to determine the mechanical and physical properties of the samples: DSC, TGA, XRD, tensile testing and DMA. Selected results that show the improvement in the piezoelectric properties of the samples due to the enhancement of the beta phase of the tailored nanofibers will be explained.

PRELIMINARY RESULTS

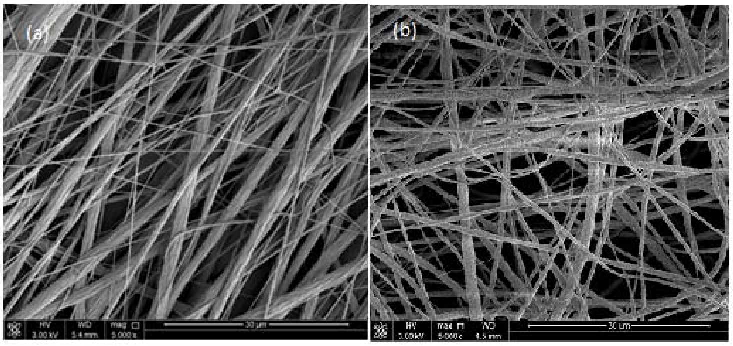

Figure A.1, SEM of PVDF composite at a)1500 RPM, AND b) 450 RPM

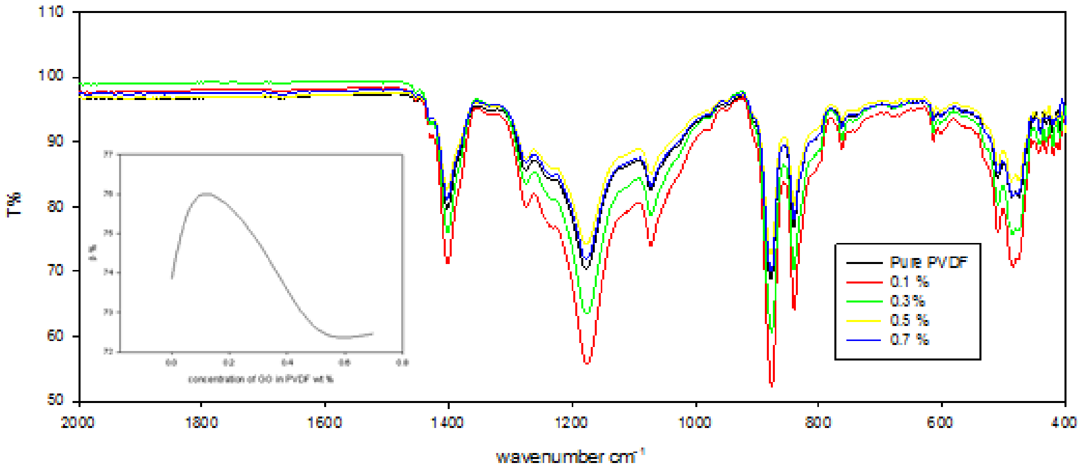

Figure A.2 48 FTIR spectra of different concentration of PVDF/GO

DISCUSSION

Figure (1) shows the effect of drum speed on the alignment of nanofibers during the electrospinning process under similar conditions. Changing the filler concentration with regard to graphene oxide shows FTIR data as in figure(2). We see an increase in β-phase content until certain concentration (0.2%)of Graphene Oxide, then decrease in β-phase content with further increase in concentration.

The percentage of β phase was calculated from FTIR data by this equation

$$\beta\% = \frac{A_\beta}{A_\beta + 1.26\, A_\alpha} \text{x } 100,$$

where A_β absorbance at 840 cm^{-1} and A_α absorbance at 760 cm^{-1} .

ACKNOWLEDGEMENTS

I would like to express my special gratitude to my advisor Prof. Mariam AlMaadeed as well as Dr.Miroslav Mrlik, and Mrs. Elizabeth Thekkethottiyil who help me a lot in my project. I thank CLU, CAM, and GPC units in Qatar University for their help in preparation and analysis of the samples.

I would also like to thank my wife and my family who supported me in finalizing this work.

APPENDIX B. SEM MICROGRAPHS OF DIFFERENT MORPHOLOGIES

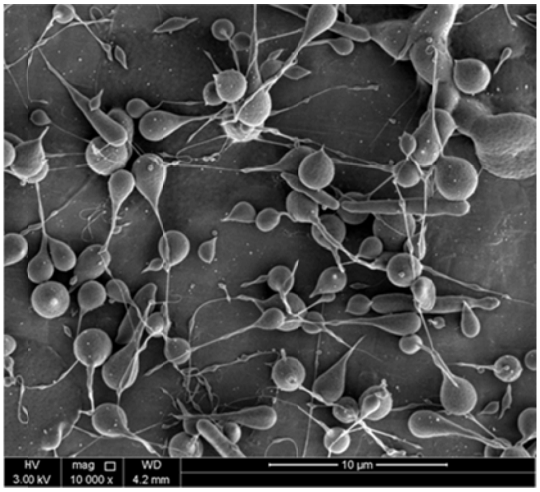

Figure B.1. SEM micrograph of 5% PVDF solution in DMF at 60 ^{o}C

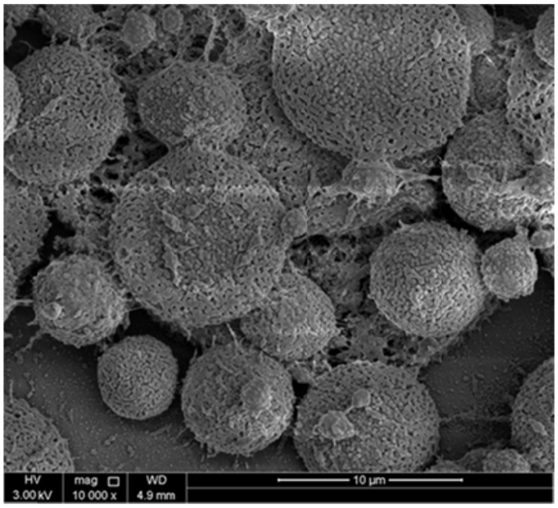

Figure B.2. SEM micrograph of 10% PVDF solution in DMF at 60 ^{o}C

APPENDIX C. HYDROPHOBICITY STUDY OF PVDF AND ITS COMPOSITES

Figure D.1(b) shows that the hydrophobicity decreased with increasing the concentration of GO in the samples prepared by a casting technique. Despite the decrease in hydrophobicity by increasing the concentration of GO in the samples prepared by electrospinning and casting, it looks as if it is controlled more by the surface morphology of the samples than the composition, so the hydrophobicity of electrospun samples was not studied in this work.

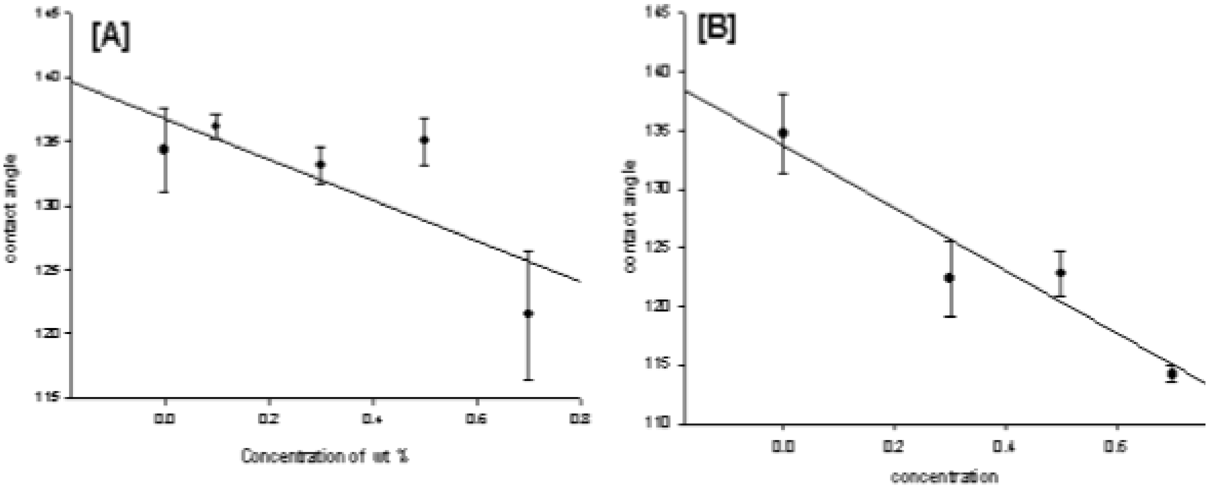

Figure C.1. Contact angle of PVDF/GO film prepared by [A] electrospinning, [B] casting and drying with air

APPENDIX D. FTIR AND UV/VIS SPECTRA OF GO

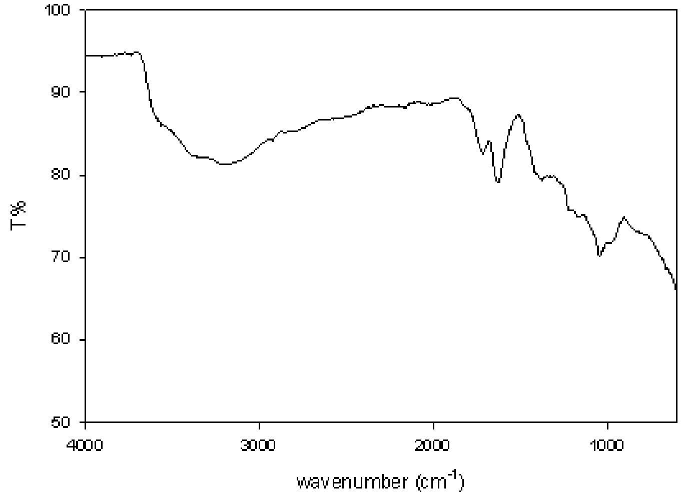

Figure D.1. FTIR spectrum of graphene oxide

Figure D.1 shows the FTIR spectrum of GO, the peaks at 1037, 1618, 1710, broad band at 3000 cm^{-1} indicate the presence of (C-O), (skeletal vibration), (C=O), and carboxylic acid and (-OH) groups respectively [86]. figure D.2 shows the UV/Vis spectrum of GO, the peaks at 232 and 297 nm could be due to the presence of conjugated bond in aromatic ring.

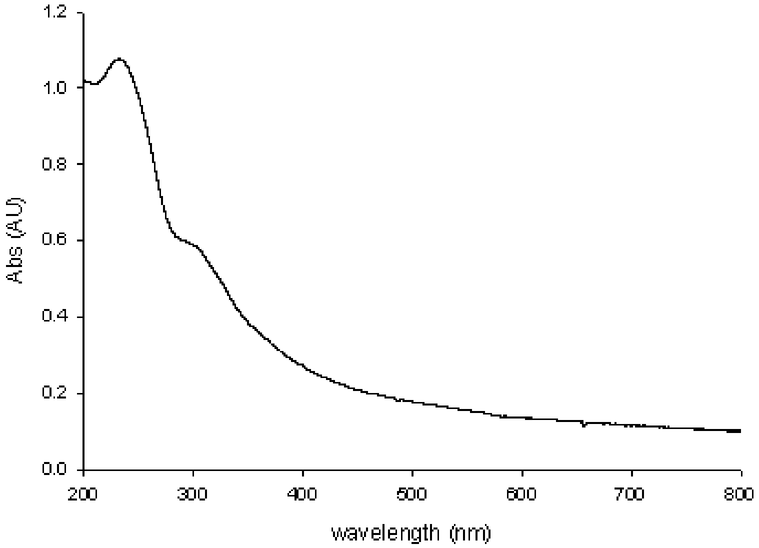

Figure D.2. UV/vis spectrum of GO solution in water